University of Szeged
Faculty of Medicine

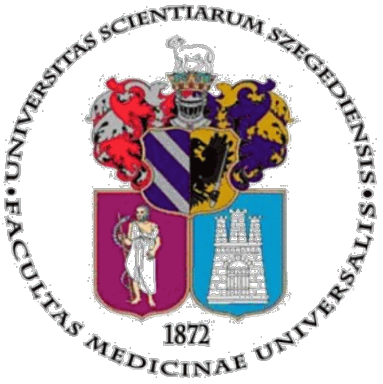

Studying physical and biochemical interactions in bacterial communities using microfabricated devices

Author:
Orsolya Sipos

Supervisor:
Dr. Peter Galajda

Doctoral Thesis

Institute of Biophysics
Biological Research Centre of the Hungarian Academy of Sciences

Szeged, 2015

List of publications

1. Publications related to the thesis:

   I . K. Nagy, **O. Sipos**, E. Gombai, A. Kerenyi, S. Valkai, P. Ormos, and P. Galajda. Interaction of bacterial populations in coupled microchambers. *Chem. Biochem. Eng. Q.* **28**, 225 (2014)

   II . **O. Sipos**, K. Nagy, and P. Galajda. Patterns of collective motion of swimming and non-swimming bacteria in microfluidic devices. *Chem. Biochem. Eng. Q.* **28**, 233 (2014)

   III . **O. Sipos**, K. Nagy, R. Di Leonardo, and P. Galajda. Hydrodynamic trapping of swimming bacteria by convex walls. *Phys. Rev. Lett.* **114**, 258104 (2015)

   IV . K. Nagy*, **O. Sipos***, S. Valkai, E. Gombai, O. Hodula, A. Kerenyi, P. Ormos, and P. Galajda. Microfluidic study of the chemotactic response of *Escherichia coli* to amino acids, signaling molecules and secondary metabolites. *Biomicrofluidics* **9**, 044105 (2015)

2. Other publications:

   I . Gy. M. Szabo, **O. Haja****, K. Szatmary, A. Pal, and L. L. Kiss. Limits on Transit Timing Variations in HAT-P-6 and WASP-1. *Information Bulletin on Variable Stars* **5919**, 1 (2010)

**Both authors contributed equally to this work.* ****Maiden name.*

"The role of the infinitely small in nature is infinitely great."

Louis Pasteur

Summary

Bacteria in their natural environment constantly interact with their local microhabitat and with other cells in their vicinity. In this work we considered cell adhesion, chemotaxis and bacterial communication, since all of these phenomena significantly contribute to biofilm formation and bacterial infections.

We studied the swimming motion of *Escherichia coli* (*E. coli*) cells near microfabricated pillars of variable size, and showed that bacterial cells are hydrodynamically trapped by convex walls of sufficiently low curvature. We found that entrapment was markedly reduced below a characteristic radius of curvature. Our results demonstrate the possibility of inhibiting cell adhesion, and thus biofilm formation, using convex features of appropriate curvature.

We used microfluidic devices to investigate how solid boundaries influence the motility patterns of flagellated swimming bacteria in high-density cultures. Using microfabricated chambers, we were able to control and stabilize the observed swimming patterns. Our results suggest that the physical features of the environment have strong effects on the swimming behavior of motile bacteria.

We constructed a flow-free microfluidic platform to study the chemotactic behavior of *E. coli* towards bacterial communication signals. We studied the effect of quorum sensing signal molecules of *Pseudomonas aeruginosa* (*P. aeruginosa*) on *E. coli* chemotaxis. Our results show that N-(3-oxododecanoyl)-homoserine lactone (oxo-C12-HSL) and N-(butyryl)-homoserine lactone (C4-HSL) are attractants. Furthermore, we tested the chemoeffector potential of pyocyanin and pyoverdines, secondary metabolites under a quorum sensing control. We found that pyocyanin is a weak attractant, while pyoverdines are repellents for *E. coli*.

We also demonstrated the usability of our novel gradient generator device in co-culturing experiments. We found that biochemical interactions between adjacent *E. coli* populations, and *P. aeruginosa* and *E. coli* populations resulted in dynamic spatial rearrangements and modulated surface adhesion of bacteria, and we showed that chemotaxis and likely intercellular signaling played a fundamental role in these phenomena.

Acknowledgements

First and foremost, I would like to give the expression of my sincere gratitude to my supervisor, Peter Galajda. He is a marvelous scientist with a never-ending curiosity about the world, who invested a tremendous amount of time teaching and introducing me into the true world of scientific research. I also have to thank his support in many other aspects of my life. He is a great friend, and a truly inspiring colleague. Without his ideas and support, this work would have never been possible.

I am especially grateful to Sandor Valkai, whose ideas, guidance and sincere friendship are tremendously valuable for me.

I also would like to thank my colleagues and friends at the Biophysics Institute for all of their efforts and support that made my work here easy and joyful. Special thanks go to Anna, Laccer, Lori, Gaszton, Andras, Laszlo, Kriszti, Orsi, Adam, Bea, Aniko and Zsofi, who really made my time at the Biophysics Institute special and unforgettable.

I gratefully acknowledge the help and support of Prof. Pal Ormos, the general director of the Biological Research Centre and the former director of the Biophysics Institute. Without his guidance and help, I would have never been able to work in Peter's group. He served as a wonderful role model of a successful scientist for me during the early stage of my career.

I am also indebted to Laszlo Zimanyi, the director of the Biophysics Institute, who is following my scientific career with great care.

I would like to thank the members of my family, especially my parents and my brother, for all of their effort, hard work and sincere love that made it possible for me to aim for a scientific career.

Finally, I would like to express my deepest gratitude to my dear husband, Maksim Sipos. His love and encouragement helped me through the hardest moments of my life. As an outstanding scientist and an exceptional person, he is the greatest inspiration in my scientific career and life.

My work was financially supported by the "Momentum" program of the Hungarian Academy of Sciences.

Contents

List of publications i

Summary iii

Acknowledgements iii

Contents v

Abbreviations vii

1 Introduction 1
- 1.1 Bacterial motility . . . 1
- 1.2 Physical interactions with solid boundaries and other cells . . . 4
  - 1.2.1 Hydrodynamic interactions with solid surfaces . . . 4
  - 1.2.2 Physical interactions between swimming bacteria . . . 6
- 1.3 Effects of environmental signals on bacterial swimming . . . 7
  - 1.3.1 Chemotaxis . . . 8
  - 1.3.2 Quorum sensing . . . 10
- 1.4 Microfluidics . . . 12
- 1.5 Aims of this study . . . 13

2 Materials and Methods 15
- 2.1 Microfabrication . . . 15
- 2.2 Cell culturing . . . 17
- 2.3 Microscopy sample preparations . . . 17
- 2.4 Microscopy . . . 18
- 2.5 Gradient characterization and model calculations . . . 19
- 2.6 Image processing and data analysis . . . 20

3 Results and Discussion 21
- 3.1 Bacterial swimming in geometrical confinements . . . 21
  - 3.1.1 Hydrodynamic entrapment of swimming bacteria by convex walls 21
    - 3.1.1.1 Microscopy experiments . . . 22
    - 3.1.1.2 Hydrodynamic model of the wall entrapment . . . 25
    - 3.1.1.3 Model predictions and experimental data . . . 27

3.1.2 Modifying the swimming patterns in dense bacterial cultures using microfluidic devices 29
3.1.2.1 Synchronized bacterial motion in high-density droplets . 30
3.1.2.2 Regulation of random bacterial swimming patterns . . . 30
3.2 Bacterial chemotaxis in microengineered chemical gradients 33
3.2.1 New microfluidic device for studying bacterial chemotaxis 33
3.2.1.1 Gradient characterization 34
3.2.1.2 Chemotaxis test experiments with confirmed chemoeffectors 36
3.2.1.3 Demonstration of chemotactic response of *E. coli* towards L-lysine 38
3.2.2 Chemotactic response of *E. coli* to quorum sensing related signal molecules 39
3.2.2.1 Canonical quorum sensing signals 40
3.2.2.2 Secondary metabolites 41
3.3 Interacting bacterial populations in microfabricated environment 43
3.3.1 Intraspecies interactions between *E. coli* populations 44
3.3.2 Interspecies interactions between *E. coli* and *P. aeruginosa* 46

4 Conclusions **50**

Bibliography **69**

Appendix **69**

Abbreviations

AHL	Acyl-homoserine lactone
BSA	Bovine serum albumin
CB	Chemotaxis buffer
DLVO	Derjaguin-Landau-Verwey-Overbeek
EDTA	Ethylenediaminetetraacetic acid
GFP	Green fluorescent protein
HSL	Homoserine-lactone
IPTG	Isopropyl beta-D-1-thiogalactopyranoside
LB	Lysogeny broth
OD	Optical density
PBS	Phosphate buffered saline
PDMS	Polidimethylsiloxane
PEB	Post exposure bake
PIV	Particle image velocimetry
RPM	Revolutions per minute

Chapter 1

Introduction

1.1 Bacterial motility

Since Anthony van Leeuwenhoek first saw and described bacteria in 1676, we have collected a considerable amount of knowledge about the elaborate world of these single cell organisms. Without bacteria, the astonishing biological diversity of Earth would not be possible. Cyanobacteria had a crucial role in the process of oxygenation of the atmosphere and the formation of the ozone layer, which enabled the various ancient life forms to migrate onto the mainlands [1]. Beside the immense influence on the ecosystem of our planet [2], bacteria have a fundamental impact on human health [3].

Microbes can form complex functional communities through vivid physical and biochemical interactions with their microenvironment and other cells, which can lead to amazingly complex social behavior that often resembles multicellularity [4]. To understand these structured, functional microbial communities, we should study the physical and biochemical cell-cell and cell-habitat interactions on the single cell and population level.

In their natural environment bacteria often encounter physical confinements and heterogenous distribution of chemical compounds. Motility offers a great advantage in these conditions, as self-propelled bacteria are able to move towards favorable habitats, even if the chemical composition of their environment is constantly changing.

The physics of motility of a microorganism in aqueous media is fundamentally different from the physics on the macro scale [5]. When an object is moving in viscous

fluid, the Reynolds number (Re) shows the ratio of the inertial forces to the viscous forces:

$$Re = \frac{\text{inertial forces}}{\text{viscous forces}} = \frac{lv\rho}{\mu} \tag{1.1}$$

where, l is the characteristic linear dimension of the object, v is the mean velocity compared to the fluid, ρ is the fluid density and μ is the dynamic viscosity of the fluid. If we substitute the characteristic values for an ordinary rod shaped bacteria, which is approximately 1 μm in diameter and 2 μm long, swimming in water at an average speed of 25 μm/s, we gain that $Re \sim 10^{-5}$. This means that microorganisms are living in low Reynolds number regimes, where viscous forces dominate, and inertial effects are negligible. When the propulsion of a bacterial cell ceases, there is no coasting in the fluid, the cell stops practically immediately.

Bacteria developed different types of swimming motility to move around their viscous drag-dominated world. Many motile bacteria use flagella to propel themselves. These are long (10–12 μm) and thin (20 nm) filaments protruding from the cellular membrane. Based on the number and arrangement of the flagellar filaments, we can distinguish polar monotrichous, multitrichous and lophotrichous bacteria, with one or more flagella at one or both poles of the cell body, and non-polar peritrichously flagellated bacteria, such as *Escherichia coli* (*E. coli*)[6]. There are also bacteria that can swim without external flagellar filaments such as *Spirochetes* [7], where the flagella are inside the periplasmic space, between the inner and outer membrane, and the rotation of the flagella compel the whole helical cell body to rotate and propel the cell forward. Bacteria also developed forms of motility on solid or semisolid surfaces, such as swarming, twitching and gliding [8]. Out of these various and diverse modes of motion we are concerned with flagellar swimming motility of *E. coli*, one of the most examined and illustrious model organism of bacterial motility [9].

E. coli is a rod-shaped peritrichously flagellated bacterium. Each flagellum is connected to a molecular motor in the cell membrane by a hook, a flexible protein structure (Fig. 1.1(a)) [10]. The flexible hook and the more rigid helical flagellum are polymers of single polypeptides, formed by hook protein (FlgE) and flagellin (FliC) respectively. Structures of the flagellar supramolecular complex embedded in the cell wall form the basal body that includes four rings (C, MS, P and L) and a rod. The torque, that is

necessary for the propulsion of the cell is generated by the MotA and MotB proteins, which are attached to the inner membrane with transmembrane helical segments. These proteins are arranged around the MS- and the C-rings. MotA is on the cytoplasmic side of the inner membrane while MotB, anchored to MotA, is mainly located in the periplasmic space [11]. The energy source of the bacterial flagellar rotary motor is the transmembrane electrochemical gradient [12, 13]. It has been shown that the rotational speed of the flagella is directly proportional to the proton motive force under physiological conditions [14].

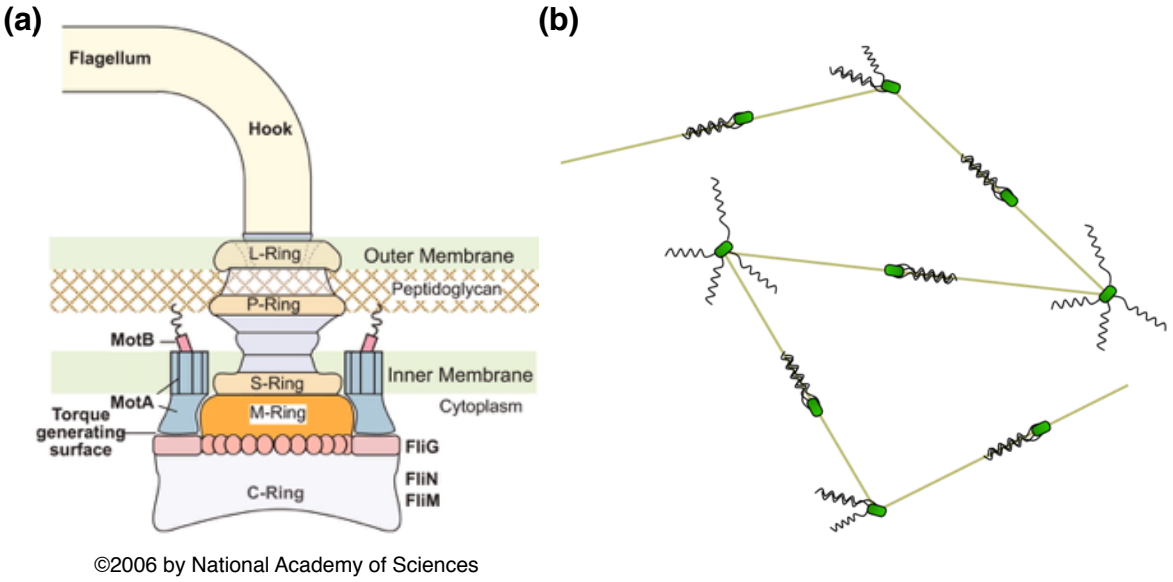

FIGURE 1.1: (a) A cartoon of the key structural components involved in torque generation in a bacterial flagellar motor (From Xing *et al.* PNAS 2006, 103(5):1260). (b) Schematic representation of the "run and tumble" type swimming motility of *E. coli*.

When the motors rotate counterclockwise the intrinsically left-handed helical filaments form a flagellar bundle that propels the cell forward very effectively. This straight swimming motion is called the "run". The average duration of a run is 1–2 seconds. If the rotational direction of any rotary motor is switched to clockwise, the corresponding flagellum would disintegrate from the bundle and undergo a "polymorphic" transformation, when the handedness and the wavelength of the filament changes. This event stops the cell and provides an opportunity to change the swimming direction due to random rotation: the cell "tumbles". These tumbling events are immediate (~ 0.1 s). The tumbling has a slight forward bias, the mean value of the angle of rotation during a tumble is 62°, instead of 90° [15]. This can be caused by the often incomplete dispersal of the flagellar

bundle. This so-called "run and tumble" motion is eventually a three dimensional random walk [16], that enables bacteria to effectively explore their environment(Fig. 1.1(b)).

The random bacterial swimming motility can be affected by numerous environmental stimuli [17–23]. In the following sections we shortly review some of those important physical, chemical and biological interactions with the local environment that can profoundly influence bacterial swimming behavior.

1.2 Physical interactions with solid boundaries and other cells

Physical and hydrodynamic interactions with the local environment and adjacent cells can profoundly influence bacterial swimming motility. In the next sections we briefly overview this topic and point out two interesting phenomena: accumulation of microorganisms near solid surfaces and emerging swimming patterns in high-density bacterial cultures.

1.2.1 Hydrodynamic interactions with solid surfaces

Bacterial habitats are often confined by physical boundaries. Collisions with these solid confinements can affect bacterial swimming behavior [24–28]. It has been observed that swimming bacteria are attracted to solid surfaces, and this phenomenon results in a notable cellular accumulation near solid boundaries [26, 29–32].

Using a tracking microscope, Frymier *et al.* observed an apparent tendency of bacteria to swim adjacent to solid surfaces, and decreased swimming speed in the vicinity of a surface [31]. The authors applied the Derjaguin-Landau-Verwey-Overbeek (DLVO) theory to the observed near-surface bacterial motion. This theory describes the interactions between colloidal particles by combining attractive van der Waals forces with repulsive electrostatic forces [33]. The observations were attributed to an emerging, overall attractive interaction potential between the bacterial cell body and the solid surface.

Further studies found that the observed accumulation of bacteria was not consistent with the predictions of DLVO theory [32]. The separation between a swimming cell body and a solid surface is greater than the expected range of electrostatic and van der Waals interactions, that act over tens of nanometers. Later it was proposed, that

while DLVO forces could be responsible for irreversible adhesion of bacteria to solid surfaces, the observed wall entrapment during swimming may have a purely hydrodynamic origin [34, 35]. Hydrodynamic effects can give rise to wall entrapment via two different mechanisms. Vigeant *et al.* proposed that when a bacterium swims next to a wall, a hydrodynamic torque would arise from the anisotropic shape of the cell body. This would tilt the bacterium towards the surface and compel the cell to follow the wall for an extended period of time. This way the cell would swim along the wall with an orientation that is not parallel to the surface. A cell that follows a solid surface would "wobble" about its equilibrium orientation, which originates mostly from the rotation of the flagellar bundle. This "wobbling" along with the rotational Brownian motion would eventually allow the cell to escape. In a fundamentally different approach of this problem Berke *et al.* estimated the flow field around a swimming flagellated microorganism using a force dipole approximation. The authors showed that purely long-range hydrodynamic interactions give rise the reorientation of a bacterial cell body parallel to a solid wall, which would lead to a subsequent wall entrapment [35].

More recently the role of hydrodynamic interactions has been questioned [36, 37]. It was suggested that collisions with a solid wall, which redirect the orientation of the cells parallel to the surface, and the effect of rotational Brownian motion are enough to reproduce the observed accumulation of bacteria in the proximity of solid walls.

Despite the extensive theoretical and numerous experimental works in the hydrodynamics of bacterial swimming, a straightforward, unambiguous and direct identification of the main mechanism responsible for wall entrapment is still lacking. All the existing models capture different aspects of the problem, and they are all capable of justifying the accumulation effects observed at flat walls.

Besides the importance of understanding the hydrodynamics of bacterial swimming, cell-surface interactions have a substantial biological importance [28]. Biofilms are multicellular (and often multispecies) communities, that develop on surfaces such as rocks, soil particles, teeth, industrial pipelines and catethers [38–41]. Surface colonization by biofilm-forming bacteria is initiated by contact and adhesion to the surface [25, 42, 43], in which hydrodynamic trapping can play a crucial role. The subsequent biofilm growth can cause highly resistant bacterial infections on medical implants and

catheters, or impaired industrial equipment [44–49]. The potential benefits of preventing biofilm formation point out the practical significance of understanding the physical mechanisms behind cell-surface interactions.

1.2.2 Physical interactions between swimming bacteria

Interactions between individuals in a group of organisms often lead to the emergence of new patterns of behavior. Such interactions on the most fundamental level can lead to the synchronization of magnitude and direction of the velocity of moving individual organisms. Emerging patterns of collective motion can be found in the living world on a wide range of scale and complexity: from the building blocks of the cytoskeleton of eukaryotic cells [50], to high-density cultures of microorganisms [51–53], to schools of fish and flocks of birds [54, 55].

The first experimental description and characterization of organized swimming patterns of bacteria was given about fifteen years ago [52], when emergence of short-lived jets and whirls were observed in a thin liquid film of *Bacillus subtilis* colonies on agar plates. Mendelson *et al.* used micron-sized beads to probe the fluid flow and characterize the swimming patterns. The authors deducted that the development of the colony structure was essentially influenced by cell motility. These observations inspired several subsequent experiments to reveal the fundamental physical and hydrodynamical interactions that govern the synchronization of the swimming behavior of bacteria in high-density cultures.

Self-concentration of *Bacillus subtilis* cells and large-scale coherent patterns were also observed in fluid droplets by Dombrowski *et al.* [53]. The local increase of concentration of cells and the formation of well-defined swimming patterns were connected with buoyancy effects, oxygen consumption and chemotaxis towards oxygen-rich regions. The authors also showed that the collective motion of microorganisms emerged due to purely hydrodynamic interactions between the cells and the surrounding fluid. The synchronization of active motion of bacteria leads to the enhancement of diffusion as it has been shown both in quasi 2D (thin films) and 3D (droplet) samples [56–58]. This can provide several benefits for the whole population (e.g. better nutrient availability or faster biochemical signal propagation). Sokolov *et al.* studied the spatial scale of self-organization

in bacterial suspensions and found a gradual increase in spatial correlation length with increasing bacterial density [59].

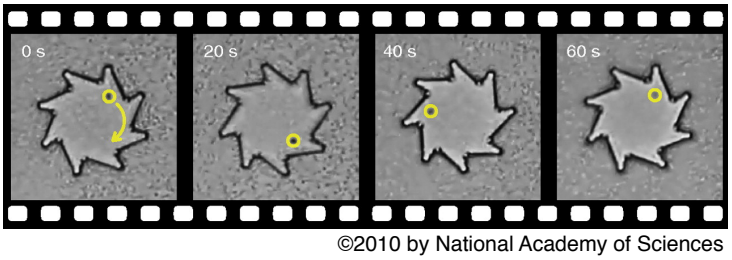

FIGURE 1.2: Bacterial driven micromotor. A nanofabricated asymmetric gear (48 μm external diameter) rotates clockwise at 1 rpm when immersed in an active bath of motile *E. coli* cells. (From Di Leonardo *et al.* PNAS 2010, 107(21):9521)

Beside the extensive fundamental experimental and theoretical work [60–64] on the physics of the collective swimming behavior in high-density bacterial cultures, engineering applications have also started to appear. A numerical simulation predicted that swimming bacteria are able to rotate microscopic wheels [65]. A year later, experiments proved the simulation and its derived model right (Fig. 1.2) [66]. Furthermore, an efficient rotation effect was seen with synchronously swimming bacteria [67]. Kasher *et al.* used microfluidic devices to study the possible applications of exploiting the motility of swimming *E. coli* cells to drive currents in well-designed microengineered environments [68]. These results foretell that we are on the way towards developing and implementing of microfluidic devices powered by microorganisms [66, 67].

1.3 Effects of environmental signals on bacterial swimming

In their natural habitat, bacteria can sense and respond to a vast range of environmental signals such as the intensity of light, nutrients, pH, temperature, osmolarity and oxygen levels [17, 18, 21–23]. Using an elaborate chemosensory system, bacteria often respond to chemical environmental clues by changing their swimming motility patterns via chemotaxis [9, 18].

On the other hand, the past decades revealed a new group of very important chemical clues for bacteria: small secreted communication signals, that profoundly affect

the behavior of microbial communities. This bacterial communication phenomenon is called quorum sensing because the concentration of the secreted signal molecules, which is proportional to the local cell density, must reach a minimal threshold level in order to elicit an appropriate response [69, 70].

In the following parts I shortly outline these two important biological processes, chemotaxis and quorum sensing, and raise the question if there are any direct interactions between these two phenomena.

1.3.1 Chemotaxis

Through chemotaxis, bacteria are able to detect concentration gradients of chemoeffector molecules and change their motile behavior according to the perceived temporal changes in the chemoeffector concentration [9, 18, 71]. In the presence of a spatial gradient of chemoeffectors, a temporal bias is introduced to the originally random walk-type bacterial swimming motility. As a result, bacteria tend to swim towards favorable environmental conditions such as higher attractant and lower repellent concentrations.

The detection of chemoeffector molecules in *E. coli* is mediated by cytoplasmic membrane receptors: methyl-accepting chemotaxis proteins (MCPs). There are five known chemotaxis sensors. The two major receptors, Tar and Tsr, are detecting mainly aspartate and serine, respectively. Out of the three other minor receptors, Tap is devoted to dipeptides, Trg to ribose and galactose, and Aer to redox potential [72]. The chemoreceptors tend to cluster at the poles of the cell body, and the function of the minor receptor complexes is dependent on their interaction with the Tar and Tsr receptors [73, 74]. The detection of the differences in the chemoeffector concentrations in the local environment is based on temporal comparisons [9]. *E. coli* is able to sense chemoeffector concentration gradients through 10 orders of magnitude via an adaptation process, which is mediated by methylation of glutamate sidechains on the receptor proteins [75].

In the chemosensory system the conversion of the environmental stimuli to a chemotaxis response is based on protein phosphorylation (Fig. 1.3) [76]. A histidine kinase (CheA) with a coupling protein (CheW) and a response regulator protein (CheY) is connected to the chemoreceptors. The kinase activity of CheA is modulated by ligand binding and the methylation level of the chemoreceptors [77, 78]. Binding repellents to

the chemotaxis receptors increases the kinase activity of CheA. CheA in its active state can phosphorylate two response regulators, CheY, a small cytoplasmic regulator protein, and CheB, a methylesterase, that can demethylate the chemotaxis receptor proteins.

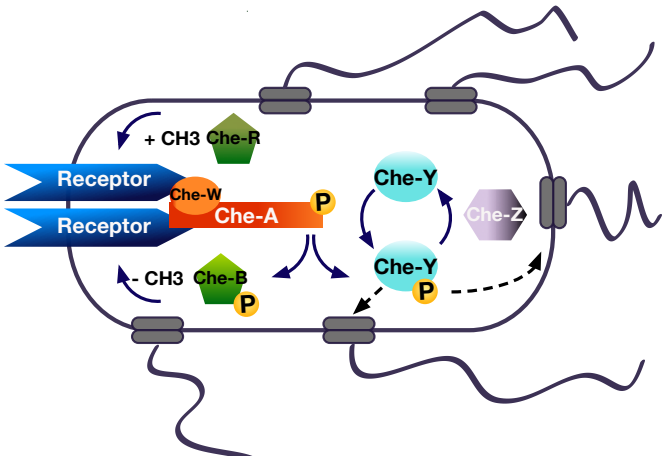

FIGURE 1.3: Schematic representation of the main components of the chemosensory pathway of *E. coli*.

When CheY is phosphorylated, a subsequent conformational change would allow Che-Y-P to bind to a flagellar motor and initiate a switch in the direction of rotation [79, 80]. As the default rotational direction is counterclockwise, this switch causes the disintegration of the flagellar bundle. The cell can change its swimming direction. To make sure that CheY-P does not affect the flagellar motor for too long after the detection of repellent molecules (making the chemotactic response very accurate), CheZ dephosphorylates CheY-P in the cytoplasm [81]. On a parallel regulatory pathway the active CheA activates the demethylation of the MCP-s, through the phosphorylation of CheB. As the receptor proteins in a methylated form stimulate the CheA kinase activity, this CheA triggered demethylation helps to decrease the activity of CheA, serving as a negative feedback loop that allows the adaptation of the phosphorelay system to repellent stimuli [82, 83]. On the other hand, during attractant binding the kinase activity of CheA is reduced. The subsequent reduced phosphorylation of CheY does not cause changes in the rotation of the flagellar motor, no "tumbles" are initiated for a while, and "runs" are lengthened. Meanwhile, the reduced phosphorylation of CheB allows a specific methyltransferase CheR to undisturbedly methylate the MCP-s, which leads to an increased activity of CheA, and a subsequent adaptation to the attractant stimuli.

In other words *E. coli* lengthen runs if currently swimming in an increasing attractant gradient, which helps it to find beneficial conditions. On the other hand, when a repellent concentration increases, there is no enhancement in tumbling rate, purely random walk is executed. As Howard C. Berg poetically expressed his thoughts about the chemotaxis response of *E. coli* [9]: " ... if life gets better, *E. coli* swims farther on the current leg of its track and enjoys it more. If life gets worse, it just relaxes back to its normal mode of behavior. *E. coli* is an optimist."

Motility and chemotaxis are common phenomena in the microbial world, and they can provide significant advantage to bacteria in various environmental conditions and biological processes. Nitrogen fixating bacteria are guided by their chemosensory system to find the optimal living conditions around legume root hairs [84]. Bacteria in the oceans use their chemotactic ability to effectively utilize transient nutrient sources [85]. Bioremediation by bacteria is often facilitated by chemotaxis [86]. Furthermore, chemotaxis also plays an important role in colonization and pathogenic bacterial infections [87–91].

1.3.2 Quorum sensing

By using quorum sensing, bacteria can coordinate their gene expression patterns on the population level in relation to the communication signal concentration in their local environment, which refers to the actual cell density [92]. At the beginning, this density-dependent gene regulation seemed to be a unique feature of a few bacterial species, but later it was found that quorum sensing is a very common phenomenon in the microbial world. Multiple quorum sensing circuits and corresponding signaling molecules have been identified in different bacteria [69, 70].

Gram-negative bacteria utilize acyl-homoserine lactons (AHLs) as signal molecules, synthesized by a LuxI-type enzyme. AHLs can freely diffuse through the cell membrane and accumulate in the extracellular as well as in the cytoplamic space. When a signal molecule binds to its cognate receptor, a LuxR-type protein, the LuxR-AHL complex binds to the promoter regions of the genes under quorum sensing control, and actives transcription (Fig. 1.4) [93]. On the other hand, Gram-positive bacteria use short peptides as communication signals, which requires an active transport system to export the signal molecules from the cytoplasm, and transmembrane receptor proteins to detect

these extracellular signals. The signal transduction occurs through a phosphorylation cascade, which activates a DNA binding protein to regulate the target gene expression [92]. There are several bacterial species that facilitate their quorum sensing gene control via the integration of multiple communication signals [94].

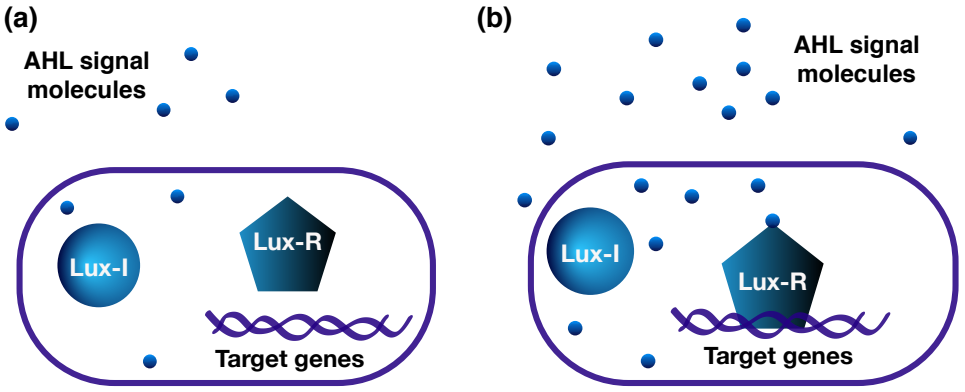

FIGURE 1.4: Quorum sensing system in Gram–negative bacteria. (a) At low signal molecule concentration no response is elicited. (b) At high signal molecule concentration (above a threshold level) the Lux-R type receptor-signal complex activates the transcription of the target genes.

Many bacterial species use the AI-2 signal molecule (a furanosyl borate diester), which is thereby considered as an interspecies communication signal [95]. The chemical vocabulary of bacteria contains numerous other molecules, with different chemical properties. *Streptomycetes* use gamma-butyrolactones as communication signals [96] and *P. aeruginosa* uses 3,4-dihydroxy-2-heptylquinolone or PQS (Pseudomonas Quinolone Signal) in addition to its AHL signals [97]. It was also shown that 3-OH palmitic acid methyl esters can act as communication signals [98], and the role of cyclic dipeptides was described in the communication of Gram-negative bacteria [99].

These signals can trigger a wide range of important biological mechanisms, such as biofilm formation, virulence, sporulation, antibiotic resistance, colony formation, exoenzyme production, cell differentiation, and antibiotic production [100–103], by coordinating the gene expression patterns of the whole bacterial population.

Most Gram-negative bacterial species with a quorum sensing system produce a characteristic set of AHLs. These chemicals are mainly treated in the literature as intraspecies communication signals. Nevertheless, it has been proved that other species are able to sense and respond to them as well. For example, SdiA was identified in *E. coli* as

a receptor protein, which can be only used for AHL signal interception, as *E. coli* does not produce any AHL molecules [104–106].

While these signaling molecules are natural clues for bacteria, it is an interesting question if they could be chemoeffectors (even for other species) at the same time. Previous studies showed that AI-2, the general interspecies communication signal has a chemoeffector potential [107], but there are no hints in the literature of the chemoeffector potential of AHLs. The relation between quorum sensing and chemotaxis seems particularly important if we consider that both phenomena play a crucial role in bacterial infections [89–91, 108–110].

1.4 Microfluidics

The study of bacterial communities was entirely based on traditional microbiological techniques until not too long ago. The traditional methods included growing monocultures on agar plates, in constantly shaken flasks, or in chemostats. It was recently revealed that the topology of the microbial habitat and the uneven distribution of nutrients or chemical signals inherently influence the behavior of microbial communities [111]. Microfabrication and microfluidic technology provide an outstanding opportunity to design and build precisely controlled microenvironments for microbiological studies.

Microfluidics is multidisciplinary scientific field, which deals with the operation and manipulation of liquids (pumping, mixing) in the spatial dimension of 1–1000 μm. Miniaturization offers many benefits in scientific research, including lower production costs, portability, decreased consumption of reagents and chemicals, and parallelization. Microfluidics became a primary technology in applications of miniaturized systems currently used in biological, chemical and medical research (PCR, single molecule DNA sequencing, lab-on-a-chip technologies, biosensors) [112]. By using microfabricated microhabitats we can obtain deeper understanding of the physical and biochemical interactions between bacteria and their local environment [113].

Initially, microfabrication technology used for chemical and biological applications was based on the already used technologies of the microelectronics industry, mostly photolithography and silicon and glass etching. These techniques are, however, relatively expensive, mostly due to the need of complex infrastructure. Furthermore, silicon is not

transparent in the visible/UV region of the spectrum, making optical imaging difficult during experiments [114]. The introduction of elastomers in microfabrication technology by soft-lithography techniques expanded the range of possibilities in biological research [112], and made it possible to create microstructures in a quick, convenient and inexpensive way by using rapid prototyping and replica molding methods [115].

Studying bacterial swimming motility and chemotaxis requires precise operation with liquids and chemical gradients on the microscopic level, in which microfluidics has already been proven to be an excellent choice [116]. In the last decade several microfluidic devices were developed for bacterial chemotaxis studies. The majority of these gradient generators rely on fluid flow [107, 117, 118]. Although, gradients can be established in these devices, in most of the cases bacteria are only exposed to the gradient for a short time (20–30 sec) as they are carried along with the flowing media. Therefore, weak chemotactic responses may not be detected in these devices. The flow may also cause shear stress on cells, which can influence their behavior. The location dependent flow velocity (e.g. a usually parabolic flow profile) in the channel may result in a hydrodynamic orientation of rod shaped bacteria, which may hinder the observed chemotactic response. The above mentioned limitations can be overcome by flow-free gradient generator devices. Two main types of these gradient generators have been developed. Some of them use flow for a short period of time in the test channel [119–121], or separately in another microchannel [122–127] to allow the chemical gradient establishment. Others rely solely on diffusion during gradient formation [128–130]. One of the biggest advantages of the flow-free devices compared to flow-based ones is that undisturbed chemotaxis response can be studied in a steady liquid medium for an extended period of time.

Using the tools of microtechnology can greatly enhance our capabilities in biological research and can lead to more accurate information and deeper understanding of the enthrallingly complex world of microbes.

1.5 Aims of this study

In this work bacterial swimming behavior is under investigation in microfluidic devices. The aim of our experiments was to understand the physical and biochemical interactions between swimming bacteria and their local environment, that may play important roles

in the development of complex microbial communities, biofilm formation and bacterial infections. We address the following questions about the physical aspects of bacterial swimming behavior:

- What is the main mechanism behind reversible wall entrapment?
- Does the surface geometry affect cell adhesion?
- How do the geometric constrictions (solid boundaries, walls, chambers) affect the swimming behavior of bacteria in high-density cultures?
- Can we shape and stabilize emerging swimming patterns by physical constrictions?

Beside physical boundaries the constant vivid interactions of bacteria with their chemical environment also influence the behavior of bacterial communities. For bacterial chemotaxis studies we aim to develop a novel microfluidic device, in which we are able to quickly establish a stable linear chemical gradient in a flow-free environment. This device can be used to study the chemotaxis response of *E. coli* towards several chemical compounds involved in bacterial communication in order to gain a deeper understanding of the role of biochemical communication in microbial communities and bacterial infections. In this thesis we focus on the following interesting biological problems:

- Can we find evidence of direct interactions between chemotaxis and quorum sensing?
- Can we use our novel microfluidic device to show chemotactic effects of canonical quorum sensing signals or molecules under quorum sensing regulation?
- Can we study the complexity of chemical communication between adjacent bacterial populations in our microfluidic device?

Chapter 2

Materials and Methods

2.1 Microfabrication

In our experiments we used polydimethylsiloxane-based microfluidic devices which were manufactured using standard soft lithography techniques [115]. Polydimethylsiloxane (PDMS) is a silicon based elastomer which is commonly used in microfluidic technology for its convenient properties. It is a non-toxic, chemically inert, biocompatible elastomer. It is optically transparent in the 240–1100 nm spectral region and permeable to non-polar gases, like O_2, N_2 or CO_2. Due to these features PDMS-based microfluidic devices are suitable for cell culturing, from bacteria to mammalian cells.

The main steps of the microfabrication process were (i) designing the microstructures, (ii) fabrication of the photomasks, (iii) production of the master molds, (iv) creating the elastomer based microdevices by replica molding [131]. Although the final physical parameters of our microfluidic chips were different, the basic procedure of the fabrication was the same for every device. We used UV-photolithography to create the master molds for the microfluidic chips. Blueprints for the photolithography masks were designed using KLayout, an open source layout editor software. The desired patterns of the microchips were printed onto emulsion film or chromium-based photomasks (JD Photo-Tools Ltd.) according to the size of the smallest features of the design. Creating chromium masks is more difficult and expensive but they can deliver details down to 1 μm, while emulsion film based transparency sheets can be used if the smallest structures are larger than $\sim$20

μm. After creating the photomasks, we prepared the master molds for the microfluidic chips.

SU-8 is an epoxy based negative photoresist which is frequently used in microtechnology, and it is an excellent material for creating master molds for microfluidic devices. Negative photoresists are light sensitive chemicals in which polymerization occurs upon exposure to light with appropriate wavelength (in the case of SU-8 it is 350–400 nm). The actual formation of the chemical bonds during polymerization happens in two steps in the SU-8 photoresist [132]. Due to the UV light exposure acid generation occurs, hexafluoroantimonic acid develops, which acts as a catalyst in the cross linking process. The actual formation of cross links in the resist occurs if the temperature is appropriately elevated during the post exposure bake (PEB). We applied 40–75 μm photoresist layers (SU-8 2015, SU-8 2050 (MicroChem Corp.)) onto 100 mm diameter silicon wafers (University Wafers, Inc.) by spin coating. The layers were soft baked on a level hot plate for 3 minutes at 65℃ and for 6–9 minutes at 95℃. After this soft bake step, the SU-8 layers were exposed to UV light (λ∼365 nm) through the photomasks by using a mask aligner equipped with a mercury lamp with an i-line filter (Newport New Illumination System, Newport Corp.). PEB was taken place right after exposure, when the SU-8 layers were baked for 1–2 minutes at 65℃ and for 6–7 minutes at 95℃. The unexposed and non-polymerized parts of the SU-8 layers were removed after PEB by immersing the wafers into SU-8 developer (MicroChem Corp.) solutions for 10 minutes.

Positive replicas of the master molds were made by PDMS (Sylgard 184, Dow Corning Corp.) casting. In order to prevent the attachment the molds to the PDMS, they were treated with (tridecafluoro-1,1,2,2-tetrahydrooctyl)trichlorosilane (Gelest Inc.) under vacuum for 4 hours. The uncured PDMS was poured onto the master molds and the devices were baked at 40–90℃ in an oven for overnight, which resulted a complete polymerization of the PDMS. The polymerized microchips were peeled off the master molds, and inlet holes were created.

Depending on the actual microchip design, the PDMS devices were bound to coverslips, using oxygen plasma treatment [133], or to $\sim$ 60 μm thick aluminium-oxide membranes (Anodisc 47, Whatman). The attachment of the microchips to the membranes was achieved by a stamping method [134], using a thin (6–10 μm) layer of PDMS. In order to create deeper chambers, we directly applied 1 mm thick layers of photoresist (SU-8

2050) onto coverslips. These samples were cured on precisely level hotplates at 95℃ for 3 days. Before the PDMS casting, these molds were also exposed to UV light, treated with SU-8 developer and silane, similarly to the above described procedures.

2.2 Cell culturing

In the hydrodynamic entrapment experiments, we used the smooth swimming *E. coli* HCB437 [135] strain carrying the pMPMA2-GFPmut2 plasmid [136]. The cell culture contained 50 μg/ml ampicillin, streptomycin and kanamycin (Sigma-Aldrich). During the correlated swimming experiments we used the *E. coli* W3110 strain [137] (bearing a lac promoter inserted together with a GFP (green fluorescent protein) encoding gene). In order to induce GFP production in the W3110 cells 1 mM of IPTG (isopropyl beta-D-1-thiogalactopyranoside) (Sigma-Aldrich) was added to the cell culture 2 hours before the experiments. The chemotaxis and the interacting bacterial populations experiments were performed using the *E. coli* HCB33 and HCB437 strains carrying the pMPMA2-GFPmut2 plasmid, and the *P. aeruginosa* PUPa3 strain [138]. The cell culturing medium was supplemented with 50 μg/ml ampicillin, and streptomycin for the HCB33 strain, and 50 μg/ml ampicillin, streptomycin and kanamycin for the HCB437 strain. *P. aeruginosa* culturing medium contained 50 μg/ml ampicillin.

Bacteria were grown overnight in 3 ml of LB (lysogeny broth) media (Sigma-Aldrich), supplemented with the appropriate antibiotics or IPTG, at 30℃ in a shaker incubator (Biosan), shaken at 200 RPM. The overnight bacterial cultures were diluted 1000 times on the morning of the experiment, and bacteria were grown at the same conditions until they reached optical density 0.5–0.9 at 600 nm (OD_{600}).

2.3 Microscopy sample preparations

For the hydrodynamic entrapment experiments a 20 μl sample of the bacterial culture was diluted 50 times in fresh LB media, containing 40 mg/ml serum bovine albumin (BSA) (Sigma-Aldrich). After the microchips were filled with the samples, the inlet holes were sealed with fast curing PDMS (World Precision Instruments Inc.), and the device was mounted onto the microscope stage.

In the correlated swimming experiments 1 ml of the bacterial culture was centrifuged (at 3000 RPM for 10 minutes) by using a desktop centrifuge (Wise Inc.). The pellet was resuspended in 10 μl of fresh LB media. This concentrated sample was loaded into the microdevice for time-lapse video imaging.

During the chemotaxis experiments bacterial cells were centrifuged (at 3000 RPM for 10 minutes, 2 times), and resuspended in chemotaxis buffer (CB) (PBS, pH 7, 0.1 mM EDTA, 0.01 mM L-methionine, 10 mM DL-Lactate, supplemented with 10 mg/ml BSA) [107]. To help the quick establishment of the concentration gradient, the studied chemoeffectors were added at half of their final concentration to the bacterial sample right before injection into the microfluidic device.

During the interacting populations experiments 1 ml of each cell culture was centrifuged (at 3000 RPM for 10 minutes) and the pellet was resuspended in 1 ml fresh LB medium, which contained 40 mg/ml BSA. In the *E. coli – E. coli* interaction experiments the observation channel and one of the reservoirs were filled with bacterial suspensions. The concentration of the cells in the observation channel was half of the initial cell concentration in the reservoir. Motility medium (10 mM PBS, 0.1 mM EDTA, supplemented with 40 mg/ml BSA) was used to fill up the other reservoir. In the *E. coli – P. aeruginosa* interaction experiments the *E. coli* cells were loaded into the observation channel, and one of the reservoirs was filled with *P. aeruginosa* cells. The other reservoir was filled with CB medium, containing 40mg/ml BSA. The cell concentration in the observation channel was half of the concentration in the reservoir, due to a 1:1 ratio dilution of the *E. coli* suspension with CB medium.

2.4 Microscopy

During all the experiments a Nikon Eclipse Ti-E epiflourescent microscope (Nikon Inc.) equipped with a 10× Plan Fluor, and a 40× S Plan Flour objective, a fluorescence filter set for GFP (Chroma Inc.), a Prior Proscan III microscope stage, and a Prior Lumen 200Pro metal arc lamp (Prior Scientific Inc.) was used for imaging. The microscope setup was controlled by the Nikon NIS Elements AR microscopy software (Nikon Inc.). During time-lapse video recording, a Rolera em-c2 digital EM-CCD camera (QImaging Corp.) was used for the hydrodynamic entrapment and correlated swimming experiments,

and an Andor NEO sCMOS camera (Andor Technology Ltd) was used for the bacterial chemotaxis and the interacting bacterial populations experiments. All the long term chemotaxis and interacting bacterial populations experiments were carried out at 30℃ in a home built cage incubator mounted onto the optical table.

2.5 Gradient characterization and model calculations

Pyranine (Sigma-Aldrich), a water soluble fluorescent dye, was used to characterize the chemical gradient in our no-flow gradient generator device. Pyranine was solved in phosphate buffered saline (PBS) at 0.1 μM and 1 μM concentrations. At the beginning of the experiments pyranine solution was loaded into one reservoir, the other one was filled with pure buffer, and the observation channel was filled with a 1:1 mixture of the buffer and the dye solution. In long term experiments the complete filling procedure was done before starting fluorescence time-lapse imaging. In order to capture the beginning of the gradient formation, we carried out short-term experiments, where we mounted the sample with filled central channel and empty reservoirs on the microscope, and we started the time-lapse imaging before the reservoirs were filled. During the dye diffusion experiments fluorescence microscopy images of the central channel were taken in 15 s intervals in the first 10 minutes, 1 minute intervals in the next 50 minutes, 5 minute intervals in the next 3 hours of the experiments and hourly afterwards. A 600 μm wide and 800 μm long rectangular area was selected at the centre of the observational channel (excluding the overlapping areas (Fig. 3.10)), and the average pixel intensity of this area was measured across the channel. In the calibration experiments we loaded the reservoirs and the main channel with pyranine solution at the same concentration. We considered the measured fluorescence intensity as a direct representation of the pyranine concentration. A two dimensional simulation was done using the "Transport of Diluted Species"model of Comsol Multiphysics 4.3a software. We simulated the gradient establishment via diffusion of the pyranine molecules, and studied the stability of the gradient over time. The 30% porosity of the integrated aluminium-oxide membrane was taken into account by using an effective diffusion constant $0.1275 \cdot 10^{-9}$ m^2/s. Because the diffusion constant of pyranine was not available in the literature, we approximated it with the diffusion constant of fluorescein, a similar fluorescent dye [139].

2.6 Image processing and data analysis

Fiji, an open source software package [140], and Matlab (MathWorks Inc.) were used for image processing and data analysis for all the experiments. In the hydrodynamic entrapment experiments time-lapse video microscopy was used to follow individual bacterial trajectories. Each video consisted of 1800 frames, and they were recorded with 10 frames per second. Cell tracking was done using the MOSAIC plugin within Fiji. The trajectories were checked, and if the algorithm made mistakes, they were manually corrected. These errors were typical when tracks crossed or cells passed each other near the walls. The trajectories were considered to be trapped by the surface of micropillars, if cells traced the surface of pillars longer than 30 frames (3 s) [141] and stayed in the 3.5 μm vicinity of the surface. During data analysis, using Matlab, the bacterial trajectories were automatically sorted and classified according to their positions, lengths and the radius of the micropillar they encountered.

We used fluorescence time-lapse video microscopy with high frame rate (60 FPS) to record the dynamic swimming patterns of bacteria during the correlated swimming experiments. Particle Image Velocimetry (PIV) was used during the analysis of the swimming patterns. The data analysis were carried out using the open-source PIVlab tool of Matlab.

Fluorescence microscopy images were taken every 5 minutes during the chemotaxis and the interacting bacterial populations experiments. Before data analysis, the raw images were cropped and background correction was performed in Fiji, using the built-in Rolling ball algorithm. During image processing we had to manually correct some manufacturing artifacts that appeared as bright spots on the fluorescence images. The spots were masked, and automatically excluded from the image analysis using Matlab. During the data analysis of the chemotaxis experiments, kymographs were generated by taking thin sections of fluorescence images of the central channel at subsequent times and plotting one below the other. These kymographs demonstrate qualitatively the differences in the dynamics of the chemotactic response to various chemoeffectors.

Chapter 3

Results and Discussion

3.1 Bacterial swimming in geometrical confinements

The physical parameters and the geometry of the environment can profoundly influence the swimming behavior of self-propelled bacteria [111]. We wanted to study these boundary-induced effects in well-controlled microfabricated environments. To that end we created precisely engineered bacterial microhabitats, where we were able to study the hydrodynamic interactions between swimming cells and nearby solid surfaces, and the influence of physical boundaries on the emerging swimming patterns in dense bacterial cultures.

3.1.1 Hydrodynamic entrapment of swimming bacteria by convex walls

Can we use the geometry of the confining boundaries to get a deeper insight into the nature of the observed accumulation of bacteria near solid surfaces [26, 29–32]? To answer this question, we studied the swimming behavior of *E. coli* cells in a PDMS-based microfluidic device. The 75 μm deep main channel of the device contained several straight walls and pillars, with different radii of curvature (20–350 μm) (Fig. 3.1). We recorded individual bacterial trajectories in the vicinity of these surfaces using fluorescence video microscopy, and we analyzed each trajectory assuming that in the presence of a hydrodynamic trapping force trajectories follow the convex curvature of the micropillars.

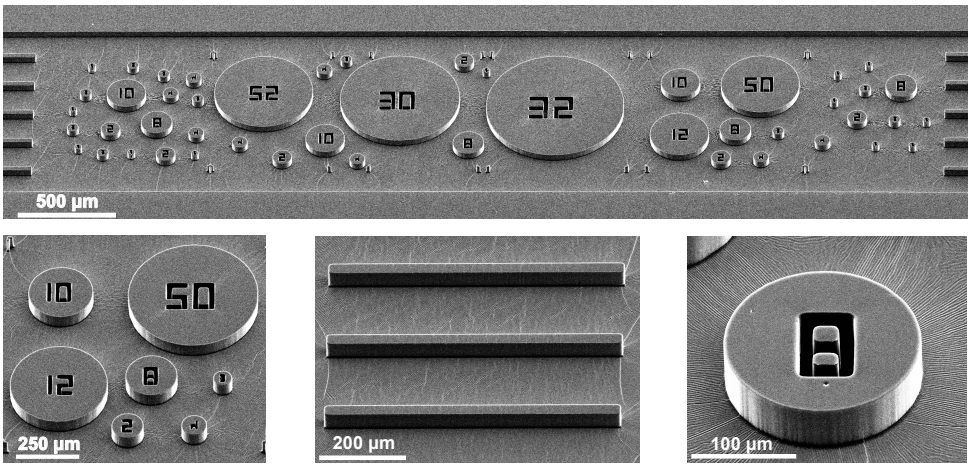

FIGURE 3.1: Scanning electron micrographs of the PDMS-based microdevice containing several micropillars. The height of the posts is 75 μm.

It is known that due to the rotation of the cell body during swimming, bacteria tend to swim in clockwise circles over flat surfaces for an extended period of time [26, 29, 31, 142–144]. To avoid the confusion of this effect with hydrodynamic trapping induced by the surface of the micropillars, we only examined bacterial trajectories with counterclockwise direction (i.e. opposite what the rotating cell body would result).

3.1.1.1 Microscopy experiments

We tracked and analyzed 1124 bacterial trajectories along straight walls and the perimeters of micropillars in our microfluidic device. We found that most of the cells followed the convex surface of the pillars (Fig. 3.2) and more than 90% of the bacteria swam along the planar walls after collision. The fraction of bacteria that followed the surface of the micropillars was 60–90%, when the radius of curvature was larger than 50 μm. Below 50 μm radius the tracing cell fraction decreased with the decreasing pillar radius. Although, we observed some bacteria following the surface of the pillars with the smallest radius of curvature (20 μm). Therefore, our findings strongly indicate the presence of a hydrodynamic trapping effect that acts on the bacterial cells swimming near a solid surface.

Tracing times, path lengths and average swimming velocities were determined around the micropillars. We found that bacteria tend to spend more time swimming around pillars with larger radii [Fig. 3.3(a)]. These findings were in accordance with our path length measurements, longer paths were measured near larger pillars. Therefore, we

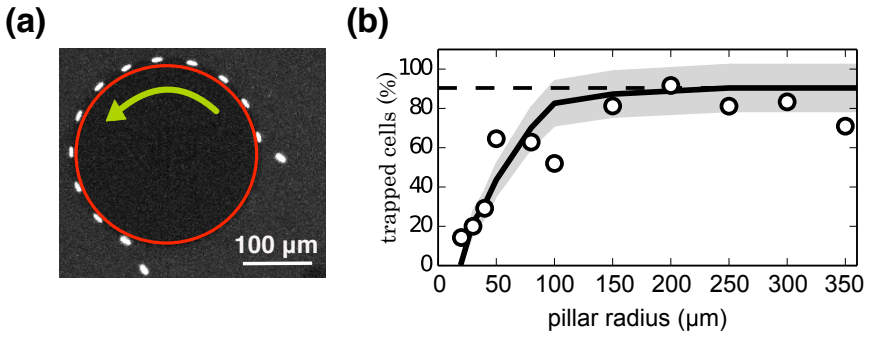

FIGURE 3.2: (a) Montage of fluorescence microscopy images of a bacterium following the perimeter of a micropillar. The arrow indicates the swimming direction. (b) The measured ratio of the cells that followed the surface of the pillars after collision (open circles) and the model prediction for the fraction of trapped cells (solid line). The dashed line represents the value for flat walls. Gray shaded area: standard deviation of the model predictions.

did not find any significant variation in the average swimming speed in the vicinity of different pillars. The average tracing speed remained in the 14–19 μm/s range for all radii of curvature [Fig. 3.3(b)], although it was constantly lower than the measured average bulk speed (24±4 μm/s).

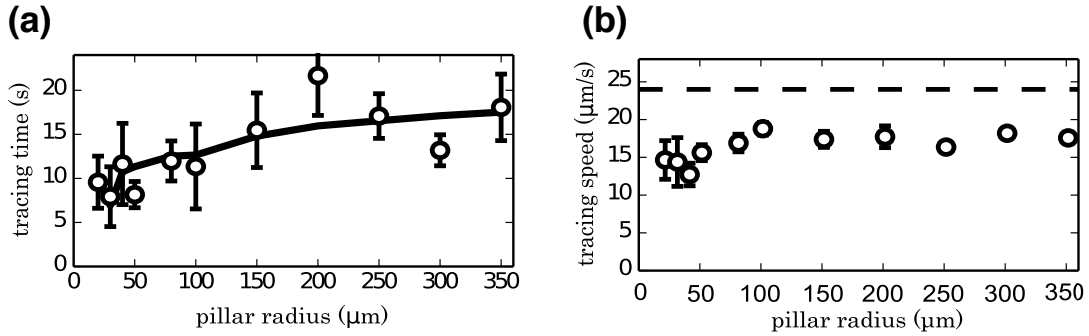

FIGURE 3.3: (a) The measured average residence times of bacteria for each pillar (open circles) and the model prediction (solid line). (b) The average tracing speed of bacteria near pillars. The dashed line represents the average speed in bulk. The error bars indicate standard errors.

We also determined the orientation of cell bodies tracing flat surfaces. We used a higher magnification (40× objective instead of 10×) during the fluorescence video microscopy recordings. Trajectories of 58 individual cells were analyzed. We found that cells usually did not align their body axis along the surface. Bacteria swam with a finite average angle to the surface plane, although, the orientation of the cell bodies fluctuated

(Fig. 3.4). The typical average angle of orientation for an individual bacterium was around 5°.

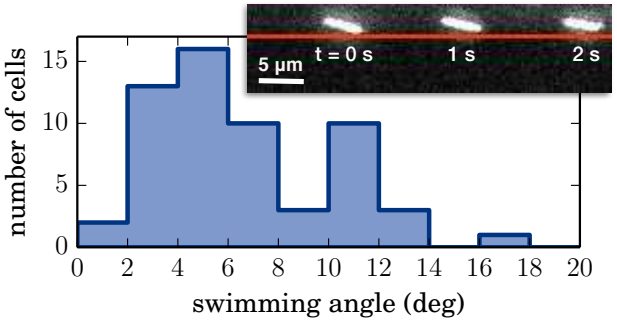

FIGURE 3.4: Histogram of the average angles of orientation of individual cells with respect to the solid wall (n = 58). The inset shows a montage of frames with a swimming bacterium near a planar solid wall. Red line shows the surface of the wall.

Our observations supported the existence of a hydrodynamic attractive force, when bacteria swim next to solid surfaces. It is an interesting question if this hydrodynamic trapping influences biofilm formation, as its first step is the attachment of planktonic cells to surfaces [25, 42]. We used our microfluidic device to study the possible effects of surface curvature on cell adhesion. We incubated *E. coli* cells in the microdevice for 18–24 hours, which allowed the cells to multiply until they filled the whole channel. Then the planktonic cells were washed out, and the adhered cells were imaged around the micropillars [Fig. 3.5(a)].

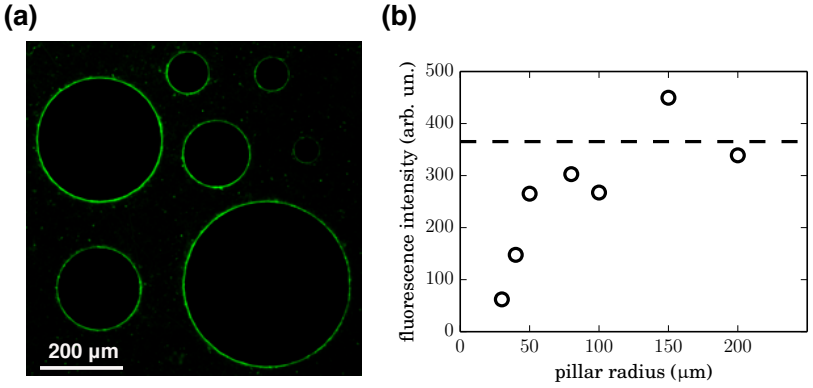

FIGURE 3.5: (a) Representative fluorescence microscopy image showing the bacterial cells adhered to the surface of the micropillars. (b) The fluorescence pixel intensity over a unit area in the vicinity (3.5 μm) of pillars and next to a planar wall. The dashed line represents the value for flat walls.

We calculated the average fluorescence intensity per pixel around the perimeter of each pillar [Fig. 3.5(b)] to measure the level of bacterial adhesion. We found that more cells stuck to the surface of pillars with larger radius. This suggests that bacteria tend to adhere to surfaces with less curvature, as the hydrodynamic trapping effect keeps them near flat surfaces for the longest period of time. The data show a similar dependence of the cell adhesion on the radius of curvature as we saw before for the cell fraction tracing the pillars and the average residence times [Fig. 3.2(b), 3.3(a)]. Our results indicate that hydrodynamic entrapment may play a role in biofilm formation via cell adhesion and surface colonization.

3.1.1.2 Hydrodynamic model of the wall entrapment

Our collaborator, Roberto Di Leonardo from Sapienza University of Rome, created a theoretical model of the physical interactions between a swimming cell and a nearby surface. Using this simple mechanistic model we can explain the existence of a characteristic pillar radius below which the trapping probability decreases. Our experimental results are in excellent agreement with the model predictions. I present briefly the physical model of the hydrodynamic trapping effect.

We model a swimmer as the combination of a spherical cell body and a helical flagellar bundle that are rigidly connected as shown in Fig. 3.6.

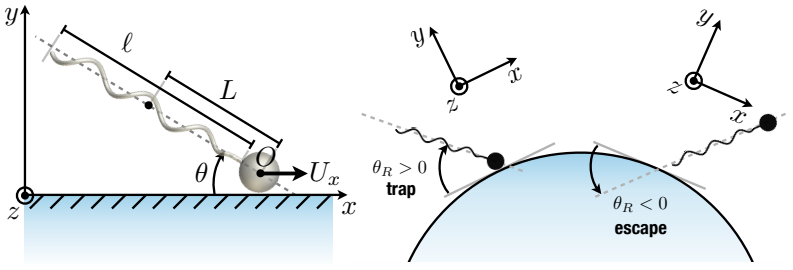

FIGURE 3.6: Schematic illustration and notation for the hydrodynamic model.

When the cell body encounters a wall a normal reaction force develops that constrains motions to the x direction. From the linearity of Stokes equation the viscous torque acting on the cell body will be linearly related to the instantaneous values of rotational and translational velocities. As long as the cell moves in contact with the wall, there are two significant velocity components we have to consider: the x component of

linear speed U and the z component of angular speed Ω. Calling T^b the z component of the viscous torque acting on the cell body we can write:

$$T^b = -C^b\Omega - B^bU \tag{3.1}$$

The first term $-C^b\Omega$ represents the viscous drag that would act on the cell body if purely rotating. The coupling term $-B^bU$ represents the viscous torque acting on the cell body when purely translating. Similarly, the torque acting on the flagellar bundle can be expressed as:

$$T^f = -C^f\Omega + B^fU \tag{3.2}$$

The coupling term is now positive, and it arises from the displacement of the flagellar bundle centre of resistance from the origin O:

$$B^f = L\gamma_\perp \sin\theta \tag{3.3}$$

where $\gamma_\perp$ is the drag coefficient determining the viscous resistance encountered by the flagellar bundle when translating in a direction perpendicular to its axis. The normal component of the emerging reaction force will not produce any torque about our origin O. In principle we cannot exclude the presence of a tangential friction component, but it will add up to the hydrodynamic component B^b. The overall system is therefore torque-free so that we can add Eqns. (3.1) and (3.2) and solve for Ω:

$$\Omega = \frac{B^f - B^b}{C^b + C^f}U = \frac{L\gamma_\perp \sin\theta - B^b}{C^b + C^f}U \tag{3.4}$$

The swimming angle θ has a stable equilibrium value θ_∞ for which $\dot{\theta} = -\Omega = 0$:

$$\sin\theta_\infty = \frac{B^b}{L\gamma_\perp} \tag{3.5}$$

where the subscript ∞ indicates that we are considering the case of a flat wall, or in other words an infinite pillar radius R. Pillar radii are always much larger than the cell size, so we can assume that the hydrodynamic resistance matrices are negligibly affected by the small wall curvature. In this situation we can take into account the finite curvature

of the pillar by moving to a reference frame that rotates around the pillar axis with an angular speed given by $-U/R$. In this new reference frame the time derivative of θ will be given by:

$$\dot{\theta} = -\Omega - \frac{U}{R} = \left(\frac{B^b - L\gamma_\perp \sin\theta}{C^b + C^f} - \frac{1}{R} \right) U \tag{3.6}$$

The stable value for θ now decreases as the pillar radius becomes smaller:

$$\sin\theta_R = \sin\theta_\infty - \frac{C^b + C^f}{LR\gamma_\perp} \tag{3.7}$$

There exists a critical value R^* for the pillar radius, below which there is no positive stable value for θ. $\dot{\theta}$ will still be negative even when $\theta = 0$, so the cell will eventually swim away from the surface (Fig. 3.6):

$$R^* = \frac{C^b + C^f}{L\gamma_\perp \sin\theta_\infty} \tag{3.8}$$

A first estimate of the critical radius can be obtained by noting that $C^f \gg C^b$ and that $C^f = \ell^2\gamma_\perp/3$ [143]. Substituting into Eqn. (3.8) we obtain:

$$R^* \approx \frac{\ell^2}{3L\sin\theta_\infty} \approx \frac{2}{3}\frac{\ell}{\sin\theta_\infty} \tag{3.9}$$

where, we used the fact that the cell length $2L$ is mostly given by the length of the flagellar bundle ℓ.

3.1.1.3 Model predictions and experimental data

As shown in Eqn. (3.5), the actual value of θ_∞ depends on B^b, a quantity that is expected to be very sensitive on the actual value of the gap between the cell and the wall. Rather than entering into the difficulties of theoretically predicting B^b, we obtained θ_∞ from our experimental observations and checked the theory by directly verifying relation (3.9). As our model predicted, we found that bacteria swam with a finite average swimming angle to the surface plane (Fig. 3.4). Substituting the observed average value for θ_∞ (5°) into Eqn. (3.9) and assuming that a typical bundle length is 7.5 μm, we find that the critical radius R^* is 57 μm, a value that is in good agreement with the observed decrease in the fraction of trapped cells below 50 μm radius.

Using the distribution in Fig. 3.4, we can also predict the fraction of trapped cells for pillars of radius R, as the fraction of θ_∞ angles whose corresponding values of R^* are lower than R. The results are shown as a solid line in Fig. 3.2(b), where we rescaled the predicted fractions to give the correct limit for infinite radius of curvature.

Equations (3.9) and (3.5) show that the critical radius for trapping does not depend on swimming speed, as expected from our purely hydrodynamic approach. This picture is consistent with our data presented in Fig. 3.3(b), where we did not find any variation in swimming speed.

Up to this point we have considered an idealised situation, where each cell is characterised by a well defined θ_∞ whose value decides whether the cell escapes from a pillar, or it is trapped around it forever. However, the actual value of the swimming angle displays large fluctuations over time due to cell wobbling and Brownian motion. Therefore, even when the average value of θ_R is positive, fluctuations can occur leading to a negative swimming angle and allowing the cell to escape from the pillar, thus we expect finite tracing times around the pillars. We saw that bacteria tend to spend more time swimming around pillars with larger radii [Fig. 3.3(a)]. We can explain this observation by noting that the larger θ_R is, the larger and more unlikely the fluctuation that is necessary to escape from the pillar. Assuming the simple linear relation $\tau = \alpha\theta_R$, we can predict the average residence time (τ) around each pillar from Eqn. (3.7) based on the values of θ_∞ in Fig. 3.4. Solid line in Fig. 3.3(a) shows the predicted average lifetimes corresponding to the best fit value for the phenomenological parameter α.

Our results demonstrate that the main mechanism for wall entrapment is hydrodynamic in nature, and it involves a finite swimming angle that keeps the cells in close contact with bounding surfaces. As a result swimming cells can be trapped by round pillars and follow the convex curvature of the pillar surface. We found that the swimming angle is gradually reduced for increasing surface curvature up to a critical radius (around 50 μm), where entrapment becomes unstable. Our observations are in excellent agreement with the predictions of our simple hydrodynamic model, that connects the critical radius for entrapment to the swimming angle near flat walls. We also showed that surface curvature can strongly affect bacterial colonization, suggesting that a suitable surface geometry

may inhibit biofilm formation. Our findings throw new light upon the importance of surface geometry in cell-surface interactions, which may be useful when designing medical implants or industrial equipment, where biofilm formation can be immensely harmful.

3.1.2 Modifying the swimming patterns in dense bacterial cultures using microfluidic devices

We have seen in the previous section that swimming behavior can be fundamentally influenced by hydrodynamic interactions between swimming cells and their surroundings. Direct physical interactions between individual cells can also shape the swimming behavior of bacterial populations, if the distance between bacteria is greatly reduced. We examined the physical characteristics of swimming motility in high-density cultures of *E. coli* in microdroplets and in a PDMS-based microfluidic chip, where we were able to control the synchronized swimming patterns of the bacteria. The 40 μm deep microdevice contained several small round chambers and merged double chambers, with inner radii of curvature of 10–50 μm (Fig. 3.7). After loading the dense cell suspension into the device, we used fluorescence video microscopy to record the dynamic swimming motility of *E. coli* cells.

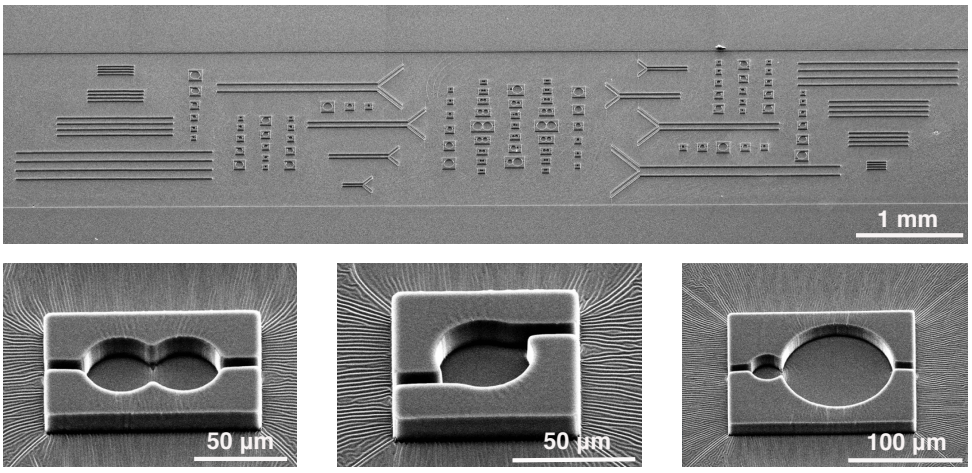

FIGURE 3.7: Scanning electron micrographs of the microfluidic device and the individual microchambers.

3.1.2.1 Synchronized bacterial motion in high-density droplets

Self-propelled bacteria in high-density cultures show a characteristic swimming behavior [52, 53, 59]. The greatly reduced distance between individual cells leads to the emergence of short-range physical interactions and synchronized swimming motion. In droplets of dense bacterial suspensions, we observed emerging whirlpools, vortices and jets, formed by groups of adjacent cells that aligned their swimming speed and direction. Without any geometrical constriction these emerging coherent formations were transient, thus, bacteria displayed fast, constantly fluctuating swimming patterns (Fig. 3.8).

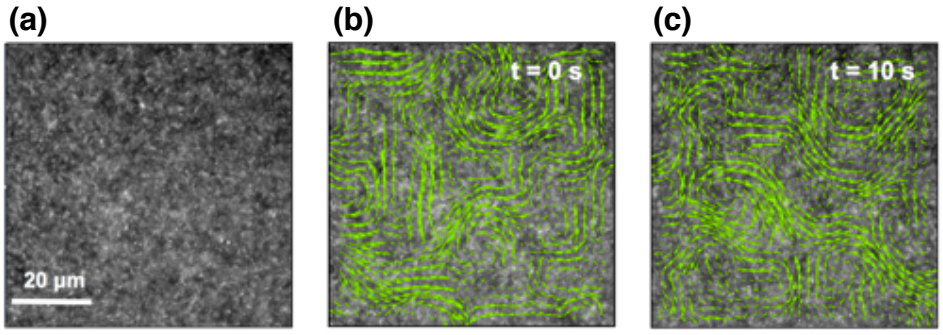

FIGURE 3.8: (a) Fluorescence microscopy image of a high-density *E. coli* suspension. (b, c) Fluorescence images of the same suspension with the calculated velocity vector field overlayed.

We used Particle Image Velocimetry (PIV) to phenomenologically characterize the emerging patterns of the synchronized bacterial motion in the droplets. We calculated the velocity vector fields for each recorded video and measured the size and the lifetime of these large-scale coherent swimming patterns. We found that the characteristic size of the transient structures was about 10–30 μm, significantly larger than the size of single bacterial cells. We also found that the observed whirlpools and jets persisted only for a couple of seconds on average (Fig. 3.8), due to the strongly fluctuating swimming motility.

3.1.2.2 Regulation of random bacterial swimming patterns

We used our microfluidic device to examine the influence of physical boundaries on *E. coli* motility in dense suspensions and to see if we can regulate the fluctuating swimming patterns using appropriately designed microstructures. The observed swimming patterns

outside the microchambers were similar to those seen in the droplets (such as in Fig. 3.8), however, in the microchambers bacteria showed stable circular motion. The velocity vector field within a double chamber on Fig. 3.9(b) clearly indicates the formation of adjacent stable whirlpools. The observed vortices persisted throughout the whole experiment (about 2 hours). We found no preference in the swimming direction of the cells, although the rotational directions of two adjacent vortices were always opposite in merged chambers [Fig. 3.9(d)]. Color-coded average velocity magnitudes within a double chamber are shown in Fig. 3.9(c) (the averaging was done over a 10 s period). We found that the maximum average velocity is achieved in a ring-like structure within both chambers. At the center and at the perimeter of the round chambers the swimming speed was reduced. Moreover, the velocity was higher in the larger side of the chamber.

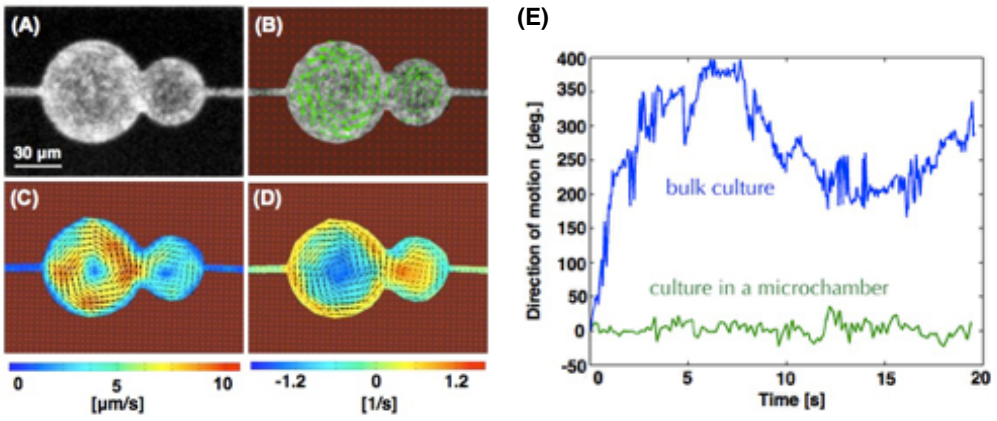

FIGURE 3.9: a) Fluorescence microscopy image of a coupled microchamber filled with a dense bacterial suspension. (b) The velocity field inside the chamber. (c) Time-averaged velocity distribution inside the chamber. (d) The vorticity of an emerging bacterial whirlpool. (e) Temporal changes in the direction of cellular motion inside and outside of a microchamber.

Based on the above-mentioned observations, we can describe the underlying mechanisms that led to these stable swimming patterns in our microchambers. As we have seen swimming bacteria move along solid surfaces after colliding with them [35, 145]. Similarly, bacteria on the perimeters of our round chambers followed and swam around the walls, which led to the observed circular motion. Due to the short-range hydrodynamic and mechanical interactions between the cells, the orienting effect of the inner walls propagated through the whole population and led to a synchronized swimming motion. These patterns were stabilized by the constant presence of the round walls. Without any

physical constriction these local physical interactions led to transient jets and vortices in free suspensions, but they resulted in a synchronized circular motion within the microchambers. The measured lower swimming speed at the perimeter of the chambers can be caused by a wall-induced friction. We have seen previously (chapter 3.1.1.1) that cells exhibit a lower swimming speed near surfaces. At the center of the vortices the reduced velocity can be associated with a required sharper turn, and a more drastic change in swimming direction. A similar effect may explain the difference of the maximum velocities in the two sides of the merged chambers with different radius of curvature.

The design of our microfluidic device allowed us to find regions between the microchambers where we could consider the motion of the bacteria unrestricted. Therefore, we were able to study the swimming behavior inside and outside the chambers in the same experiment. We examined a maximum velocity region within a chamber with 60 μm inner radius, and an open area outside this chamber at 60 μm distance from any other confining walls. We calculated the average velocity direction at two 12 μm $\times$12 μm areas. Figure 3.9(e) shows that the stabilizing effect of the geometric constraint of the walls resulted in the suppression of both the fast and slow fluctuations and irregularities of the original swimming pattern.

In our experiments we showed how geometric constraints and solid boundaries alter the swimming behavior of microorganisms. We were able to stabilize, shape, and characterize the emerging bacterial vortices inside microfabricated chambers. The development and implementation of microfluidic devices powered by microorganisms [66–68] are at an early stage, but this is a promisingly growing scientific field. The encouraging results show the compelling possibilities of these hybrid microengineered devices, where useful energy can be extracted from the random motility of dense bacterial cultures in well-designed microfabricated environments. Our results show that the structure and geometry of such microdevices may have a deep impact on the distribution and the swimming dynamics of bacteria, which fundamentally determine the usability of such applications. Furthermore, as synchronized motion is also observed for various living organisms on various scales, our results demonstrating the effect of geometrical confinement may have more general implications.

3.2 Bacterial chemotaxis in microengineered chemical gradients

As we have seen in the previous sections the swimming motility of bacteria is essentially influenced by the physical and hydrodynamic interactions with their local environment and adjacent bacterial cells. Beyond these physical interactions, chemical and biological signals can also alter bacterial swimming behavior. Bacteria can sense and respond to various chemical compounds [17, 18, 21–23]. As natural environments are often chemically heterogenous, bacteria usually encounter these signals in form of chemical gradients, which allow chemotactic bacteria to change their motility patterns according to the spatial distribution of these compounds. Our aim was to build a novel microfluidic device, in which we can generate precise chemical gradients and to study chemotactic response of *E. coli* to canonical quorum sensing signals and quorum regulated molecules.

3.2.1 New microfluidic device for studying bacterial chemotaxis

We designed and fabricated a new flow-free chemical gradient generator microfluidic platform for bacterial chemotaxis studies. The device consists of two PDMS layers and a porous membrane, which is inserted between them (Fig. 3.10). The upper layer contains two ~ 45 μl trapezoid-shaped reservoirs, in which chemoeffector and buffer solutions can be loaded. The lower layer includes the ~ 0.4 μl observational channel for studying the chemotactic response. This central channel is 40 μm deep, 1.2 mm wide and 1 cm long.

Two overlapping areas connect the observational channel and the reservoirs (Fig. 3.10). If a chemical concentration difference is applied between the two reservoirs, a steady linear chemical gradient develops across the main channel via these overlapping areas.

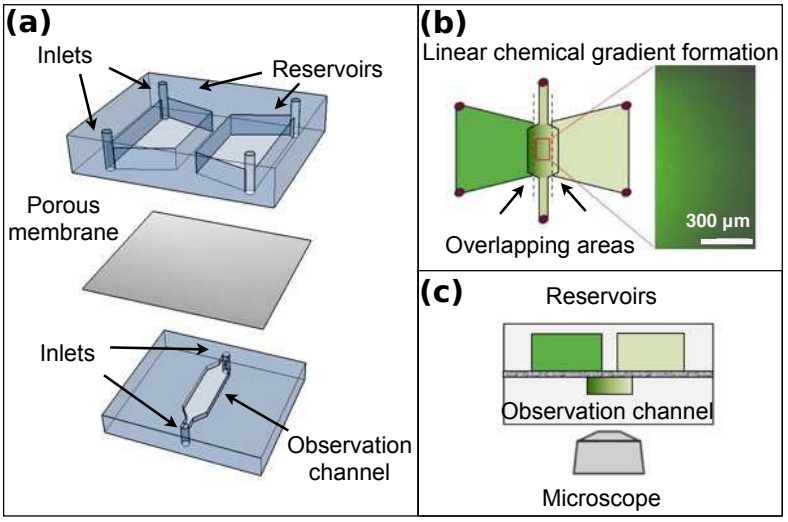

FIGURE 3.10: Schematic representation of the gradient generator microfluidic device (not to scale). (a) A perspective view showing the three sandwiched component of the device. (b) Top view of the device. The inset shows a fluorescence microscopy image of the central channel with a pyranine concentration gradient. (c) Cross sectional view of the device showing the observation of the channel from below (as in an inverted microscope).

3.2.1.1 Gradient characterization

We characterized the chemical gradient in the observational channel using pyranine, a water soluble fluorescent dye. Our measurements showed that the concentration gradient profiles were very close to linear. Figure 3.11 shows the concentration profiles of pyranine solutions across the main channel after an hour of the gradient formation. A linear fit provided r^2 values of 0.9907 and 0.9766 in case of 100 nM and 1000 nM pyranine solutions. In our microdevice the magnitude of the gradient can be precisely controlled by changing the absolute concentrations in the reservoirs (Fig. 3.11).

We used a finite element analysis in Comsol to model the gradient inside the main channel. The model utilized the full 3D geometry of the microdevice and the diffusion properties of pyranine. The model calculations provided slope values for the concentration profiles of -69.72 ± 0.005 pM/μm and -749.1 ± 0.005 pM/μm for 100 nM or 1000 nM pyranine concentrations, respectively. The measured slope values were -61 ± 0.6 pM/μm and -818.5 ± 11.7 pM/μm, which are in a good agreement with the model calculations.

We studied the formation and stability of gradients on various timescales. In short term experiments we filled the central channel with 50 nM pyranine solution and sealed the inlet and outlet holes of the channel. After starting the time-lapse recording we filled

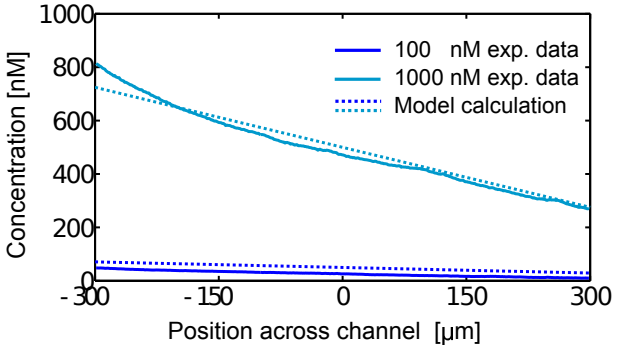

FIGURE 3.11: Concentration profiles of pyranine solutions across the central channel. Solid lines: 100 nM and 1000 nM pyranine solutions loaded in the left reservoir. Dashed lines: results of model calculations.

the left and right reservoirs with 100 nM pyranine and buffer solution, respectively, and sealed the inlet/outlet holes of the reservoirs. Fig. 3.12(a) shows the dye concentration across the width of the central channel at various times. After filling the reservoirs a linear concentration profile formed that changed little after 3 minutes. This is in a good agreement with the results of model calculations shown in Fig. 3.12(b). The slope of the concentration profile obtained by linear regression is plotted in time in Fig. 3.12(c). The graph demonstrates that the gradient formed quickly and stabilized in about 3 minutes after the reservoirs were filled. Subsequent fluctuations in the gradient were within 10%.

Flow-free gradient generator devices are suitable for long term experiments, because the developed gradient can exist for an appropriately long time. We tested the persistence of the gradient in our microfluidic device, by creating a concentration gradient with 100 nM pyranine solution and monitoring its decay over time for 72 hours. We found that the equilibration process between the two reservoirs was adequately slow due to the large volume of the reservoirs compared to the central channel and the limited overlapping areas. The drop in the gradient was only about 15% within 24 hours (see Fig. 3.12(d)).

Our results showed that in our new microfluidic gradient generator device we are able to quickly generate (in less than 5 minutes) and precisely control linear chemical gradients. We were able to maintain nearly the same gradient for at least 24 hours. Our experiments also demonstrated that our device is suitable for fast temporal manipulation

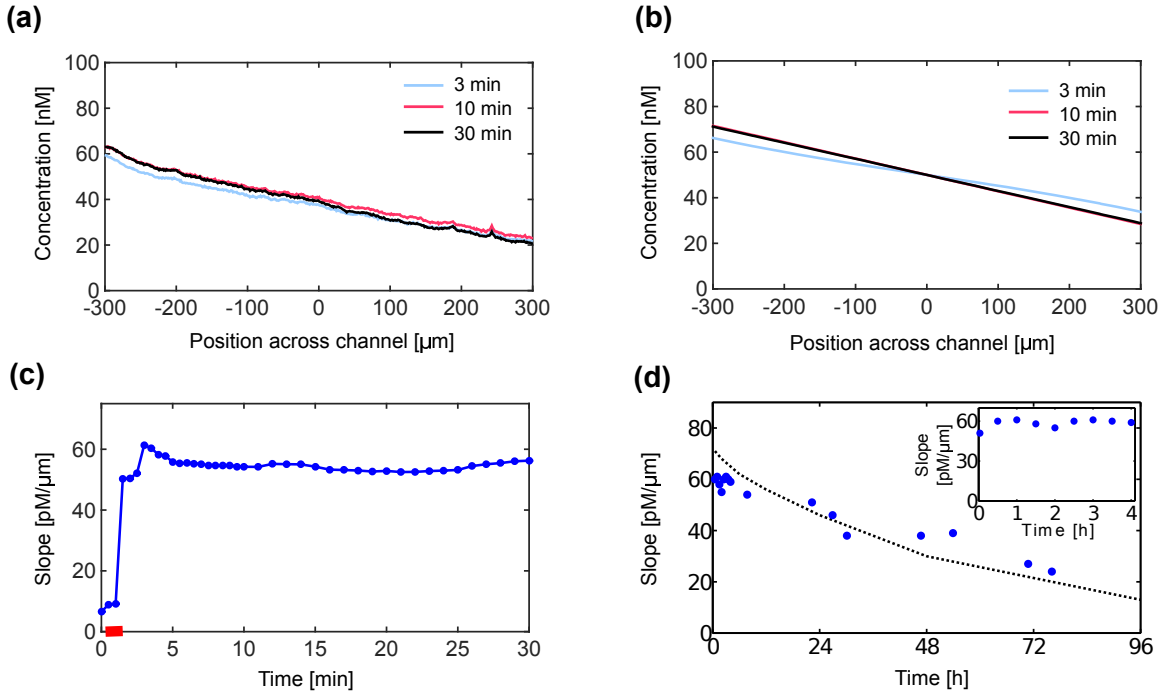

FIGURE 3.12: (a) Concentration profiles of the pyranine solution across the central channel at different times. The times indicated were measured after filling both reservoirs. (b) Model calculations of the concentration profiles of the pyranine solution across the channel at different times. (c) Short term change of the concentration gradient after filling the device. The thick red line on the x axis indicates the time needed to fill both reservoirs. (d) Change of the concentration gradient in the device in time on long timescales. Solid circles: slope of the linear concentration profile in the experiments. Dashed line: result of model calculation.

of existing gradients. By quickly changing the content of the reservoirs, the gradient in the central channel may be altered in minutes.

3.2.1.2 Chemotaxis test experiments with confirmed chemoeffectors

We demonstrated the usability of our device in chemotaxis experiments with well-known chemoeffectors for *E. coli*. We used fluorescence video microscopy to follow the motile response of fluorescent *E. coli* cells exposed to L-aspartate at maximum concentration of 100 μM, which is a strong chemoattractant and nickel, Ni^{2+} ions from $NiSO_4$ at maximum concentration of 250 μM, which is a repellent. At the beginning of the experiments bacteria spread homogenously across the central channel, but within minutes they started to move towards and away from the attractant and the repellent, respectively. After about

8–10 min almost all bacteria moved to the high aspartate, or low Ni^{2+} concentration side of the central channel (Fig. 3.13(a,b)).

In order to quantitatively characterize the observed chemotactic responses, we introduced the asymmetry index A. The index correlates with the bacterial spatial distribution in the central channel, and helps to analyze the dynamics of the chemotactic response and precisely compare the effects of various chemoffectors. A 1200 μm wide and an 800 μm long rectangular shape area was selected on each frame of the time-lapse videos. These areas were divided into two equal parts, corresponding to the two halves of the observation channel: the high concentration side and the low concentration side. Average pixel intensities were calculated on both halves of the gray-scale fluorescence images. These intensities were denoted by I_+ on the high concentration side, and by I_- on the low concentration side. Then the asymmetry index was calculated by the following equation:

$$A = \frac{(I_+ - I_-)}{(I_+ + I_-)}. \tag{3.10}$$

Choosing the nomenclature this way we get positive or negative A values for positive or negative chemotactic responses, respectively. The value of A may vary between -1 and $+1$, with the extreme cases of all cells being on the low or high concentration side of the channel.

Figure 3.13(c) shows the calculated asymmetry indeces (A) over time in the chemotaxis test experiments. The fast positive chemotactic response towards L-aspartate and the cellular accumulation on the high concentration side are clearly demonstrated as A increased quickly and maintained a positive value on the longer timescale (solid blue line in Fig. 3.13(c)). In the case of $NiSO_4$ A dropped below zero quickly and stabilized around -0.5 (dashed green line in Fig. 3.13(c)). The difference between the two chemotactic responses in dynamics and magnitude is clearly indicated by A. During the control experiments we followed the spatial distribution of wild-type cells in the absence of chemoeffector gradient (solid red line in Fig. 3.13(c)) and non-chemotactic cells in the presence of L-aspartate gradient (dashed blue line in Fig. 3.13(c)). The bacteria stayed evenly distributed across the channel and did not show any chemotactic response during these experiments (yielding a near zero A value).

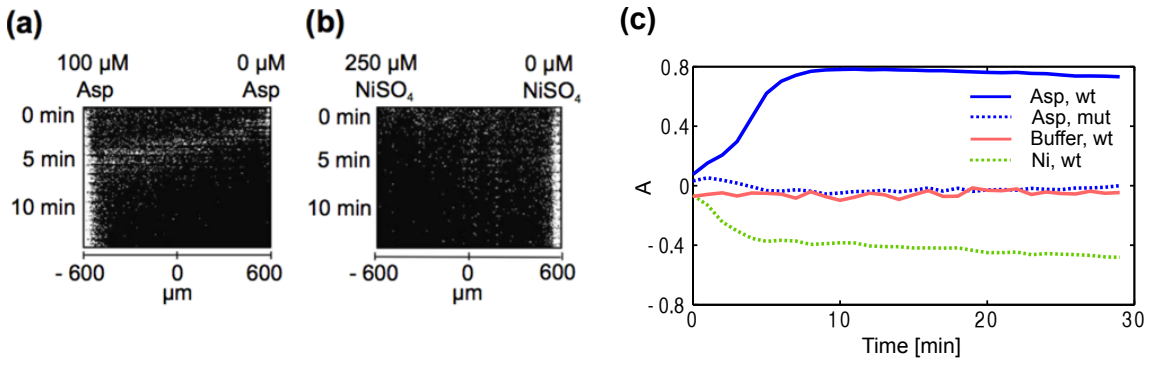

FIGURE 3.13: (a,b) Kymographs showing the temporal change of the spatial distribution of chemotactic bacteria across the channel in (a) an L-aspartate (a strong attractant) gradient, (b) a $NiSO_4$ gradient (Ni^{2+} is a strong repellent). (c) Asymmetry index (A) for bacteria in various chemical gradients. Solid blue line: chemotactic (wt) bacteria in aspartate gradient, dashed blue line: non-chemotactic (mutant) bacteria in aspartate gradient, solid red line: chemotactic bacteria in the absence of chemoeffector gradient (in buffer), dashed green line: chemotactic (wt) bacteria in nickel gradient.

In the above mentioned experiments the observed chemotactic responses happened on a longer timescale than the gradient formation. This indicates that in our device we are able to capture the dynamics of the chemotactic response itself that is not limited by a slow gradient formation. Overall, our results demonstrate the usability of our microfluidic platform in chemotaxis studies.

3.2.1.3 Demonstration of chemotactic response of *E. coli* towards L-lysine

After proving the usability of our novel microfluidic device in chemotaxis experiments, we wanted to test if we can detect very weak chemotaxis responses, that are untraceable with traditional methods. We tested two amino acids, L-lysine and L-arginine, that were considered neutral for *E. coli* based on previous capillary chemotaxis assays [146].

We tested the chemoeffector potential of L-lysine at maximum concentration of 100 mM, using the same conditions as in the mentioned capillary assay experiments. We observed a slow accumulation of the cells on the high lysine concentration side of the central channel. However, this response was much slower than the effects of strong chemoattractants. The asymmetry index indicates that after 1.5 hour there were more bacteria by 30% on the high lysine concentration side of the main channel (Fig. 3.14).

Both the degree of cellular accumulation and the characteristic timescale suggest a mild chemotactic response to L-lysine by *E. coli*.

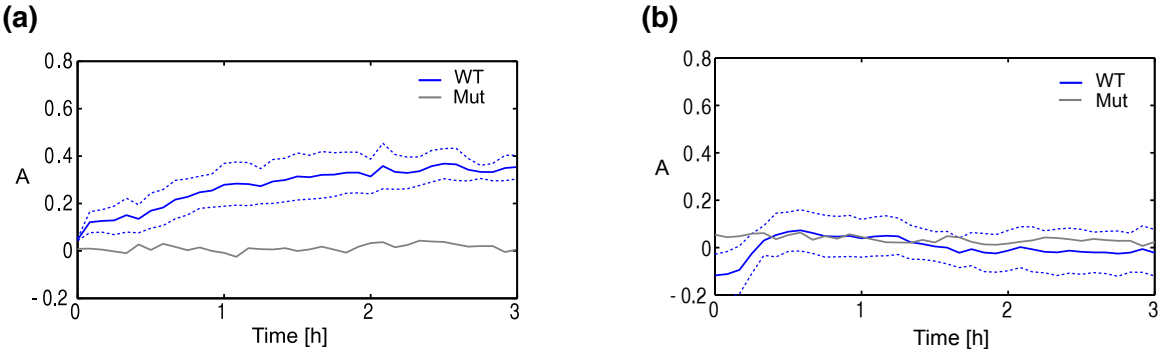

FIGURE 3.14: Asymmetry index for *E. coli* bacteria in amino acid gradients. Continuous blue line: average response of chemotactic cells. Dashed lines: standard error. Continous grey line: response of non-chemotactic cells. (a) Bacteria in lysine gradient. (b) Bacteria in arginine gradient.

The other tested amino acid was L-arginine at maximum concentration of 100 mM. We did not see any accumulation of the cells on either side of the central channel: the spatial distribution of the bacteria stayed homogeneous. The value of the asymmetry index remained near zero during the 3 hour long experiments (Fig. 3.14). Thus, our results support the previously shown neutrality of L-arginine in *E. coli* chemotaxis. In the control experiments, when we exposed non-chemotactic bacteria to the same lysine and arginine gradients, we found no detectable cellular accumulation in the main channel (Fig. 3.14).

Our test experiments showed the usability and reliability of our device during long-term chemotaxis experiments. Due to the flow-free nature of this microfluidic platform and the stable linear gradient in the central channel, we believe the device is suitable for demonstrating weak bacterial chemotactic responses. Our results showed that the amino acid L-lysine acts as a weak attractant, while L-arginine does not induce a chemotactic response in *E. coli*.

3.2.2 Chemotactic response of *E. coli* to quorum sensing related signal molecules

Bacteria can use a wide range of chemical compounds as communication signals, which at the same time can act as chemoeffectors. Through quorum sensing bacteria can alter

their gene expression patterns according to the local cell density. On the other hand, chemotactic response towards chemoattractants can lead to locally dense subpopulations. Therefore, it is an interesting question if these mechanisms interact on some level, i.e. if the density dependent quorum sensing mechanism affects cell density itself through chemotaxis by signal molecules acting as chemoeffectors. Since *E. coli* biofilm formation is affected by the SdiA receptor in the presence of certain AHL molecules [106], it is interesting to study the chemoeffector potential of these compounds.

3.2.2.1 Canonical quorum sensing signals

The two main quorum sensing systems of *P. aeruginosa*, the Las and Rhl systems, employ N-(3-oxododecanoyl)-homoserine lactone (3-oxo-C12-HSL) and N-(butyryl)-homoserine lactone (C4-HSL) signal molecules, respectively. We tested the chemoeffector potential of these quorum sensing signals on wild-type *E. coli* cells. The experiments were repeated 3–5 times both for the C4-HSL and the oxo-C12-HSL measurements. Wild-type *E. coli* cells were exposed to C4-HSL gradient in our microfluidic device with maximum concentration of 100 μM. Similar AHL concentrations were measured in *P. aeruginosa* biofilms [147]. The bacteria started to accumulate on the higher concentration side of the central channel immediately at the beginning of the experiment. The asymmetry index shows that after an hour the asymmetry in cell distribution reached its maximum value (A=0.4). Then a slow rearrangement started, and after 6 hours the original homogeneous distribution of cells was restored (Fig. 3.15(a)). Our results show that *E. coli* exhibits a strong but transient chemotactic response to C4-HSL, and some sort of adaptation mechanism or conditioning terminates this response after several hours.

We found a very similar, but considerably weaker chemotactic response of *E. coli* bacteria in oxo-C12-HSL gradients with maximum concentration of 100 μM. Similarly to the chemotactic response towards C4-HSL, we found an initial positive chemotactic response, which was followed by a slow leveling off of the spatial distribution of cells (Fig. 3.15(b)). The small maximal value of the asymmetry index (A=0.2) indicates a definite, but very mild positive chemotactic response. The maximum cellular accumulation took place after an hour, at about the same time for the two different signal molecules. In the control experiments using non-chemotactic mutant bacteria, no accumulation of cells

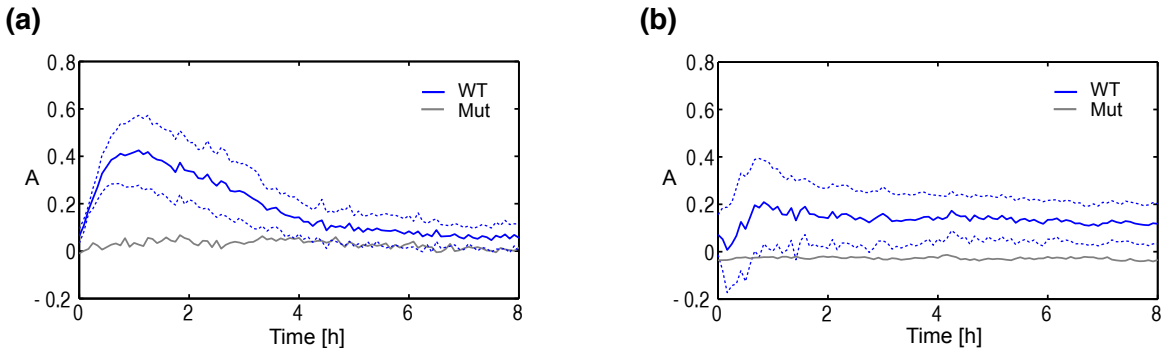

FIGURE 3.15: Asymmetry index for *E. coli* bacteria in AHL gradients. Continuous blue line: average response of chemotactic cells. Dashed lines: standard error. Continous grey line: response of non-chemotactic cells. (a) Bacteria in C4-HSL gradient. (b) Bacteria in oxo-C12-HSL gradient.

was observed on either side of the central channel (Fig. 3.15). Interestingly, the observed positive chemotactic responses towards both compounds seem to be transient and diminish or considerably weaken after a few hours. The above mentioned results suggest that there are similar mechanisms behind these chemotactic responses, however further studies are needed to explore the molecular background (e.g. receptors and signal transduction molecules involved).

3.2.2.2 Secondary metabolites

Secondary metabolites can also act as intercellular signals, and their production is often regulated by quorum sensing. The secretion of pyocyanin, a well-known secondary metabolite and virulence factor of *P. aeruginosa*, is regulated by the quorum sensing system. Pyoverdines are extracellular siderophore molecules involved in iron scavenging produced by *P. aeruginosa*. It has been previously proposed that pyoverdines can also act as communication signals in a mechanism called pyoverdine signaling [148], which is related to virulence. Furthermore, pyoverdine biosynthesis is also affected by quorum sensing [149]. As chemotaxis and quorum sensing often play important roles in virulence factor production and bacterial infections, we wanted to test if pyocyanin and pyoverdines have any chemotactic potential.

Chemotactic *E. coli* cells were exposed to a pyocyanin gradient, where the highest pyocyanin concentration was 50 μM. We chose this concentration in agreement with previous reports of concentrations of purified pyocyanin extracts from cell cultures [150]. We

found a mild positive chemotactic response of *E. coli* towards pyocyanin (Fig. 3.16(a)). The asymmetry index shows that after 30 minutes, approximately 60% of the cells accumulated at the higher concentration side of the channel (A=0.2), then the cells started to slowly spread out (Fig. 3.16(a)). Based on our results we can say that pyocyanin is a weak chemoattractant for *E. coli*. It has a much lower chemotactic potential than aspartate, nickel, or C4-HSL, but the detected response is still comparable with lysine or oxo-C12-HSL.

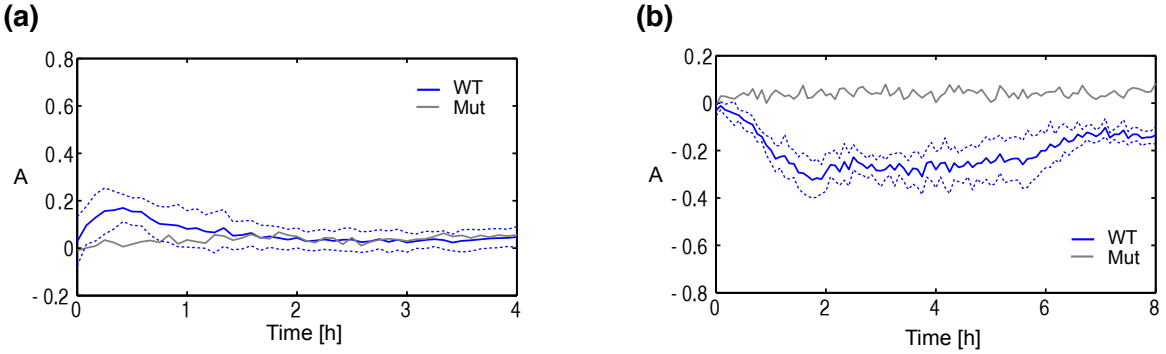

FIGURE 3.16: Asymmetry index for *E. coli* bacteria in secondary metabolite gradients. Continuous blue line: average response of chemotactic cells. Dashed lines: standard error. Continous grey line: response of non-chemotactic cells. (a) Bacteria in pyocyanin gradient. (b) Bacteria in gradient of pyoverdines.

We also studied the chemotactic response of *E. coli* to pyoverdines. We used 20 μg/ml as maximal concentration. Similar concentrations were measured previously in cell culture supernatants [151]. We observed a prolonged but weak negative chemotactic response of *E. coli* to pyoverdines. Bacteria accumulated on the lower concentration side of the channel in the first two hours of the experiment, and this asymmetric distribution was maintained for approximately 5 hours (Fig. 3.16(b)). Then cells started to spread out across the whole channel, but a visible portion of the cells stayed near to the low concentration side even after 8 hours. The asymmetry index shows that approximately 65% of the cells swam away from the high pyoverdines concentration side of the channel. Therefore, we can claim that pyoverdines are mild chemorepellents for *E. coli*. Although, the chemotactic response seems to weaken after a few hours the accumulation of cells is more prolonged compared to the case of pyocyanin. When non-chemotactic mutant cells were used during the control experiments, bacteria stayed equally distributed over the channel in the case of both tested compounds, no accumulation occurred (Fig. 3.16).

The observed chemotactic response to pyocyanin was transient and very similar to the response to the tested AHL signal molecules. We found a more prolonged, but still temporary negative response of *E. coli* to pyoverdines. It is an interesting question what leads to such transitional responses. It is known that adaptation mechanisms alter the sensitivity of chemoreceptors and span the useful concentration range in which chemotaxis works. However, it has not been demonstrated that an adaptation-like process would lead to temporal chemotactic response. Further studies are needed to reveal the exact mechanism behind the observed chemotactic responses to L-lysine, AHLs, pyocyanin and pyoverdines. For example it is not known if any of the four typical chemosensory proteins of *E. coli* has an affinity to these compounds. Although, it is known that the SdiA receptor in *E. coli* interacts with AHLs, it has not been shown that this affects chemotaxis.

3.3 Interacting bacterial populations in microfabricated environment

Cell-cell communication plays an important role in functional multispecies communities in nature [70, 152]. Beside the known quorum sensing signaling molecules (homoserine lactones and oligopeptides [153]), bacteria use toxins (antibiotics and bacteriocins [154]), antimicrobial peptides [155], amino acids [156], exopolysaccharides [157], or metabolic waste products (such as indole [158]) as communication signals. These chemical signals have a key role in the communication of bacterial populations, interacting subpopulations, and complex population dynamics [111]. We performed co-culturing experiments and showed that these complex biochemical interactions shape the spatial distribution of neighboring bacterial populations.

The setup of our flow-free gradient generator microfluidic device provides the opportunity of co-culturing different bacterial strains in the reservoirs and the central channel and studying their chemical interactions. The populations in the different chambers are physically separated from each other, but chemically coupled through the porous membrane in the device. In this configuration linear gradients of signal molecules and other secreted biochemical factors may form through the central channel. Due to the gas permeability of the PDMS, cell cultures growing in the microdevice are continuously

provided with oxygen from the atmosphere [159, 160]. The physical aspects make our microfluidic device a versatile experimental platform, where we can study the chemotactic response of bacteria to various chemical compounds, as well as we can culture cells inside the separate compartments on the long term and study their interactions through secreted chemical signals. The fast action of the device ensures that chemical factors released by one culture in one of the compartments have an almost immediate effect on the neighboring culture. This may be especially important in the case of those chemoeffectors which are only produced transiently [161].

3.3.1 Intraspecies interactions between *E. coli* populations

In our microfluidic device (Fig. 3.10) we cultured *E. coli* bacteria in one reservoir and in the central channel at the same time to study the interactions between the two distinct *E. coli* populations. Non-fluorescent chemotactic *E. coli* bacteria in nutrient rich LB medium was loaded into one reservoir. The other reservoir was filled up with motility medium, which lacks carbon resources, but contains essential salts for the cells to maintain swimming motility for several hours. The central channel contained fluorescent chemotactic *E. coli* bacteria in a 1:1 mixture of LB and motility medium.

The multiple dynamic rearrangements of the spatial distribution of bacteria in the central channel was clearly captured by the kymograph of a representative experiment (Fig. 3.17(a)), as well as by the plotted asymmetry index (Fig. 3.17(c), blue solid line). In parallel, we observed a monotonic increase in the overall fluorescence intensity suggesting an increasing cell number during the experiments. Bacteria immediately started to accumulate on the high nutrient concentration side of the central channel (Fig. 3.17(a)), and after 20 minutes nearly all cell moved to that side. This asymmetric cell distribution was steady for 90 minutes, and it was caused by the nutrient concentration gradient across the channel. LB is a nutrient rich medium, containing aspartate and serine (well-known chemoattractants for *E. coli* [15]) which might induce this positive chemotactic response. After about 90 minutes, we saw a rapid, synchronized relocation of cells to the other side of the central channel (Fig. 3.17(a)). The majority of cells crossed the channel, however, there were non-motile bacteria stuck to the surface of the microchip that stayed near the other *E. coli* population in the reservoir. The spatial distribution of the cells is also

shown in Fig. 3.17(b), where the average pixel intensity on the images (corresponding to the indicated experimental times) are plotted as a function of the distance from the midline of the channel.

We carried out control experiments with non-chemotactic *E. coli* cells to verify if chemotaxis plays a role in the spatial rearrangement of the *E. coli* population in the central channel (Fig. 3.17(c), grey solid line). We did not observe any bacterial accumulation on either side of the channel during the whole experiment. However, a slight increase in the fluorescence intensity was measured on the originally nutrient rich side, suggesting the growth rate was location dependent due to the uneven distribution of available nutrients across the channel. This finding shows that there was no complete nutrient depletion in the reservoir, which contained the non-fluorescent *E. coli* population. In other control experiments, where the nutrient rich medium did not contain bacteria, we also observed the initial accumulation of chemotactic wild-type cells on the nutrient rich side of the central channel, although, the quick relocation did not happen.

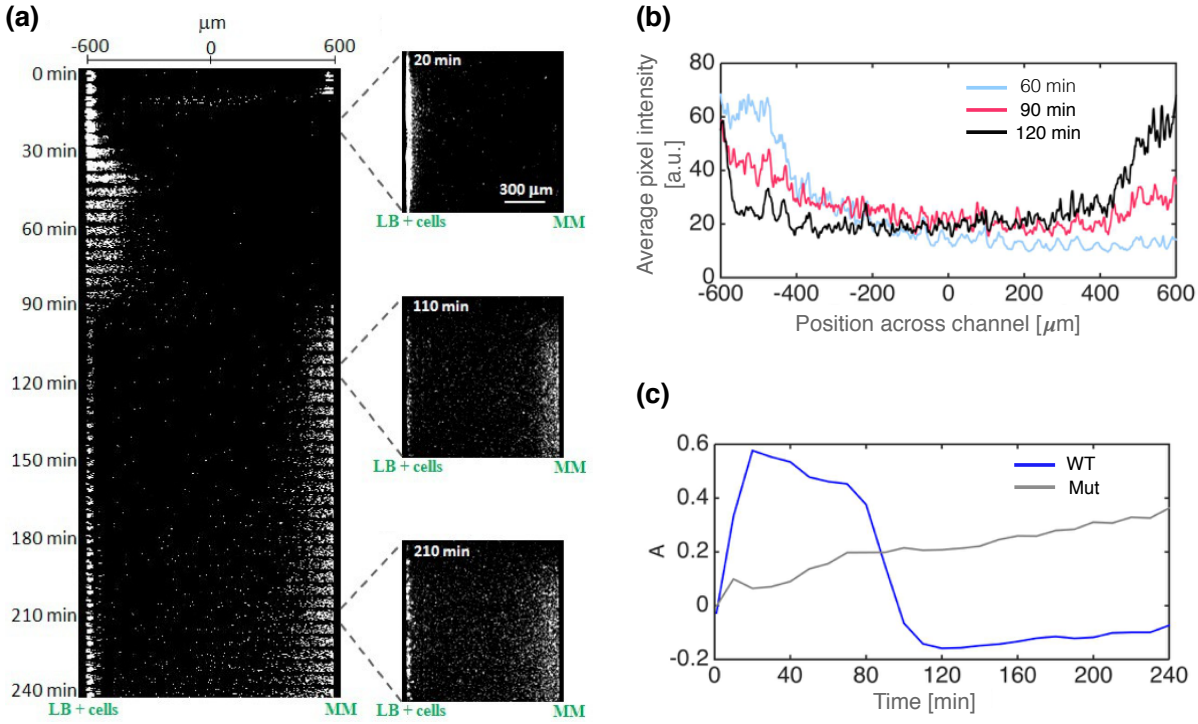

FIGURE 3.17: (a) Kymograph of a typical 4-hour experiment. Background corrected fluorescence images of the observation channel at representative time points (20 min, 110 min, 210 min). (b) Average intensity profiles measured across the observation channel at representative time points (60 min, 90 min, 120 min) of the experiment. (c) Temporal variation of the asymmetry index calculated for the wild type (blue line) and non-chemotactic mutant (red line) *E. coli* populations.

During the time course of the experiment, the nutrients were consumed and metabolic byproducts were released in the originally nutrient rich reservoir. There are several secreted products of *E. coli*, such as ethanol, acetate, and indole, which accumulate in batch cultures and can act as chemorepellents. For example, a similar repulsion phenomenon of *E. coli* populations has been observed on agar plates using the chemical in plug method [162]. The exact chemical signal inducing the negative chemotactic response is not known, but we speculate that indole may be a good candidate. It is a product of tryptophan metabolism, and it is produced by *E. coli* and many other Gram-positive and Gram-negative bacteria. It has been suggested that indole is an intercellular and inter-species signal molecule [163, 164]. *E. coli* start to produce indole in the early exponential phase under nutrient rich conditions, and it may accumulate in concentrations of about 0.6 mM [165]. At this concentration, indole is a repellent for *E. coli* [107, 162]. Furthermore, at this concentration indole does not seem to affect growth, much higher concentrations (>2 mM) are necessary for growth inhibition [106, 166].

All the above mentioned results from other works seem to support the possibility that indole accumulated in the reservoir with the *E. coli* population and induced a negative chemotactic response, resulting in the second migrational event in the later phase of the experiment. This, however, does not exclude the possibility that other chemical compounds (such as the above mentioned ethanol, acetate) play a role in the observed chemotactic response. Interestingly, our results suggest that during bacterial growth in high density cultures the secreted secondary metabolites, such as indole first can act as repellent, forcing cells to find new resources, secondly if the cell density is very high, the same secreted product can affect bacterial growth, turning down the growth rate of the population, and providing advantage for the whole population to survive.

3.3.2 Interspecies interactions between *E. coli* and *P. aeruginosa*

In the previous sections we have seen that through chemotaxis *E. coli* is able sense and actively respond to several communication signals of *P. aeruginosa*. What kind of a chemotactic response is expected, when the chemical content of the environment contains a mixture of these secreted signals? We addressed this question by co-culturing *E. coli* and

P. aeruginosa cells in our microfluidic device and studying how the swimming behavior of an *E. coli* population can be influenced by a neighboring *P. aeruginosa* population.

In the beginning of the experiments *P. aeruginosa* cells in LB medium were loaded into one reservoir, while the other one was filled with CB medium. The central channel was loaded with *E. coli* cells in 1:1 mixture of the two different media. After the assembly of the device we mounted it onto the microscope stage, and we started fluorescence time-lapse video microscopy measurements.

The *E. coli* population showed a dynamic spatial rearrangement, somewhat similar to that was observed between the interacting *E. coli* populations. However, we found distinctive differences between the two experiments on the time scale of the chemotactic response and the level of cell adhesion. In the first phase of the experiment *E. coli* cells accumulated adjacent to the *P. aeruginosa* population (Fig. 3.18(a,b)). Since a nutrient gradient formed in the central channel, probably the cells moved along this attractive gradient. After two hours the cells were fully aggregated at this side of the channel. We observed that the majority of the *E. coli* cells right next to the *P. aeruginosa* population adhered to the surface of the microdevice. However, after about 4 hours a small planktonic subpopulation migrated away from the adhered, sessile subpopulation (Fig. 3.18(a,b)). Interestingly the adhered *E. coli* cells showed a very high fluorescence intensity, higher than expected based on the cell number, that made the evaluation of the asymmetry index in this experiment impossible. Therefore, we decided to use the average fluorescence intensity across the width of the main channel to represent the dynamics of the spatial distribution of the *E. coli* population in the observation channel.

We carried out control experiments with non-chemotactic *E. coli* cells (Fig. 3.18(c)). The bacteria did not accumulate next to *P. aeruginosa* population in the first phase of the experiment, however, a slight gradual increase in the adhesion of the cells was observed too. We did not see any en masse migration of a motile subpopulation either. This result shows that the initial accumulation of the *E. coli* cells adjacent to the *P. aeruginosa* population, as well as the subsequent transmigration require chemotactic capability. We observed a slight variation of cell density across the width of the channel. This is due to a differential growth effect (the spatial variation of the growth rate) that is the consequence of the existence of a nutrient gradient in the channel, showing that there was no complete nutrient depletion in the reservoir with the *Pseudomonas* population. Such a differential

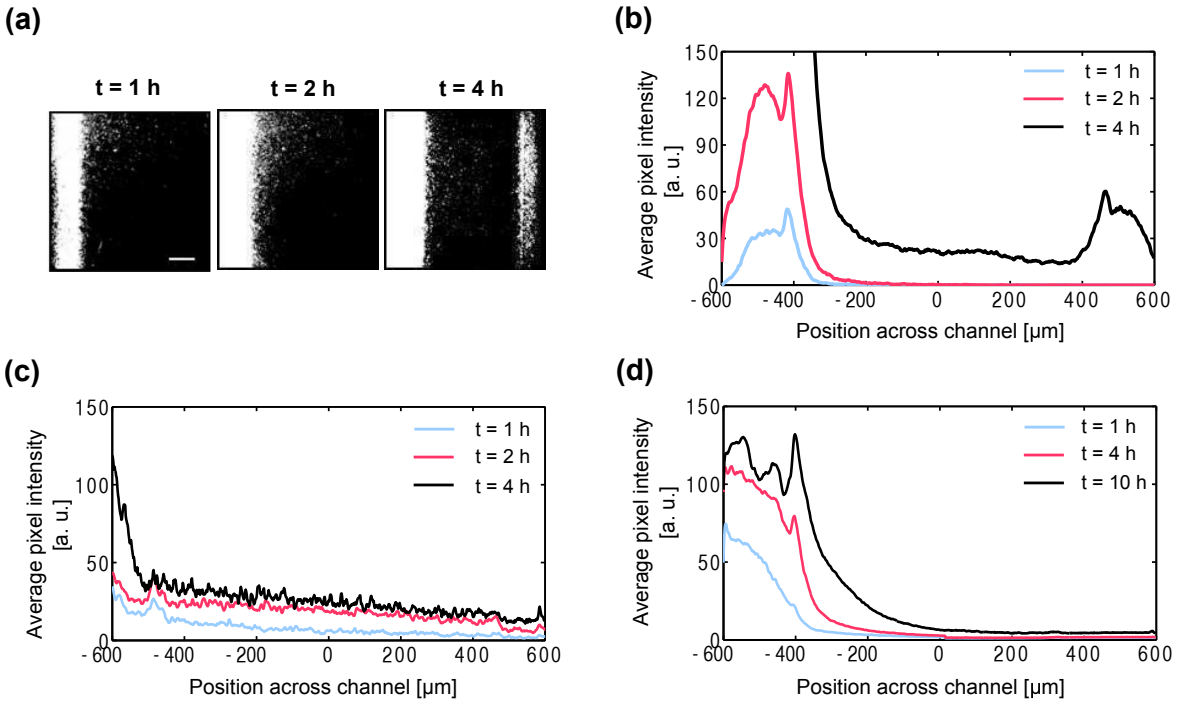

FIGURE 3.18: Co-culturing experiments showing the interaction of adjacent populations. (a) Fluorescence microscopy images of the *E. coli* culture in the channel in the *P. aeruginosa* – *E. coli* co-culturing experiment at different times. The scale bar is 200 μm. (b) Average pixel intensity across the width of the channel representing the distribution of *E. coli* bacteria at different times. (c) Average pixel intensity across the width of the channel representing the distribution of non-chemotactic *E. coli* bacteria at different times. (d) Average pixel intensity across the width of the channel representing the distribution of *E. coli* bacteria at different times for the control experiment, where cell–free pure LB medium was loaded into the left reservoir.

growth can be observed for the chemotactic cells too, although, there it is mostly covered by the strong chemotactic response.

In other control experiments we loaded blank LB media into the one reservoir without the *P. aeruginosa* cells, while CB media was on the other side, and chemotactic *E. coli* cells were in the central channel (Fig. 3.18(d)). As expected, we saw an initial accumulation of the cells due to the nutrient concentration gradient, but the subsequent transmigration to the other side of the channel did not occur. This result rules out the possibility that the migration away from the nutrient rich side of the channel is caused by the growing *E. coli* population itself, and supports the idea that the presence of the *P. aeruginosa* population was necessary for the second migration event in our original experiment.

We assume that the planktonic *E. coli* cells exhibited negative chemotaxis in response to compounds secreted by the *P. aeruginosa* bacteria. *E. coli* can detect and respond to numerous metabolic products and communication signals produced by *P. aeruginosa*, such as pyocyanin, pyoverdines, AHLs, diketopiperazines [167], Pseudomonas quinolone signal [168]. Beside of their crucial role in functional multispecies microbial communitites, these active compounds can also have chemoeffector potential, as we have seen in the case of AHLs, pyoverdines and pyocyanin. In addition to pyoverdines, which were proved to be repellents for *E. coli*, there could be other unidentified chemoeffectors that could initiate the observed negative chemotactic response. On the other hand, some of these secreted chemical compounds can act as attractants, just as the AHL signals or pyocyanin, thus, in our co-culturing experiments probably we observed a net chemotactic response to these products with opposite chemoeffector potentials.

We observed an increased cell adhesion next to the high-density populations in the reservoirs both of the *E. coli* – *E. coli*, and the *E. coli* – *P. aeruginosa* co-culturing experiments. However, the level of the adhesion was much larger in the second case. Our observations confirmed the importance of secreted extracellular signaling molecules in cell adhesion, and as a next step, biofilm formation. It was shown before that *E. coli* is able to detect AHLs through SdiA receptor protein, which regulates the expression of biofilm formation related genes [106]. Although, the concrete effect of the AHL signal molecules secreted by *P. aeruginosa* was not yet tested on *E. coli* biofilm formation. On the other hand, there must be other processes that played role in the observed increased adhesion in the *E. coli* – *E. coli* co-culturing experiments, because *E. coli* cannot secrete acyl-homoserine lactones.

Overall, we could say that our microfluidic device is a suitable and versatile experimental platform to investigate the complex behavior of multispecies microbial communities. Our findings show that interacting microbial populations could profoundly affect each other through biochemical interactions. Our microfluidic device proved to be an ideal platform for studying the dynamic pattern formations, which are a result of the interplay between several chemical clues, even opposing, attractant or repellent effects. In the light of the results we obtained about the chemotactic responses of *E. coli* to pyoverdines, pyocyanin and AHL gradients, a population level interaction between adjacent bacterial colonies may be quite complex.

Chapter 4

Conclusions

Physical interactions between individual cells and their surroundings or adjacent cells can profoundly shape the swimming behavior of self-propelled bacteria. Moreover, bacteria can detect and actively respond to numerous environmental signals, such as nutrients, temperature, pH, toxins, secreted metabolic compounds, communication signals. These bacterial communication signals can connect multiple microbial communities, and immensely influence microbial swimming behavior too. We used microfabrication technology to create precisely controlled microhabitats, where we studied the physical, chemical and biological interactions between single cells and microbial communities.

We studied the swimming motility of *E. coli* cells near microfabricated convex surfaces to elucidate the main mechanisms behind wall entrapment. Our results demonstrate that the main mechanism for wall entrapment is hydrodynamic in nature, and it involves a finite swimming angle that keeps the cells in close contact with bounding surfaces. We found that the entrapment by convex walls is progressively reduced below a characteristic radius of 50 μm. We also showed that the curvature of the surface can strongly affect colonization by biofilm forming bacteria. Our results suggest that a suitable surface geometry may inhibit biofilm formation.

We also studied the intrinsic features of the correlated swimming motility of *E. coli* bacteria in high-density bulk cultures and in microfabricated chambers. We described the dynamic swimming patterns in bulk cultures phenomenologically, using Particle Image Velocimetry techniques. We found that whirlpools, vortices, and jets emerge, translate and disappear on a timescale of seconds, and the characteristic size of the large-scale

coherent structures is about 10–30 μm. We managed to stabilize the originally fluctuating swimming patterns of *E. coli* by using suitably designed microchambers, and we evaluated the regulated swimming motility.

Beside the mechanical and hydrodynamic interactions, chemical signals can also deeply impact the swimming behavior of microorganisms. Bacteria usually encounter these compounds in the form of chemical gradients in their natural environment. We built a new microfluidic platform to study the chemotaxis response of *E. coli* bacteria to several chemical compounds, such as amino acids, quorum sensing signaling molecules, and secondary metabolites.

In our novel PDMS-based flow-free gradient generator device we are able to quickly establish stable chemical concentration gradients and maintain them for almost 24 hours. We demonstrated the usability of this device with well-known chemoeffectors. We showed that the amino acid L-lysine acts as a weak attractant, while L-arginine does not induce a chemotactic response by *E. coli*. We found that C4-HSL and oxo-C12-HSL, the canonical quorums sensing signals of *P. aeruginosa* are chemoattractants for *E. coli*. The chemotactic response towards these compounds were found to be transient and diminish or considerably weaken after a few hours. We have also tested two types of secondary metabolites produced by *P. aeruginosa*, which are under quorum sensing regulation. We showed that pyocyanin is a weak attractant, while pyoverdines are repellent for *E. coli*. These chemotactic responses are also transient, similarly to the response to AHLs. Further studies, applying molecular biology techniques, are needed to fully understand the mechanisms behind these transient chemotactic responses and reveal the molecular background of the detection and response to the communication signal molecules.

In multispecies bacterial communities interspecies interactions may have an important role in the organization and function of the community. To demonstrate this on a basic level, we performed co-culturing experiments in our new microfluidic device, and we showed that complex biochemical interactions shape the spatial distribution of neighboring bacterial populations.

We showed that metabolic products or signaling molecules (i. e. ethanol, acetate, indole), secreted by an *E. coli* population growing in nutrient rich environment, act as chemorepellents and increase the cellular adhesion of a neighboring *E. coli* population. We also demonstrated that a *P. aeruginosa* population produces chemical compounds

that vastly increase cellular adhesion of an adjacent *E. coli* population. On the other hand, unidentified chemorepellents were secreted by the *P. aeruginosa* population that induced negative chemotactic response of a small planktonic subpopulation of *E. coli*. Our results suggest that communication signal molecules and secondary metabolites connected to quorum sensing could be among the potentially important chemicals that may act throughout the induction of a chemotactic response between adjacent bacterial populations.

In this work we examined several seemingly distinct biological processes, such as cell adhesion, chemotaxis and bacterial communication. As all of them significantly contribute to biofilm formation and bacterial infections, our findings help us to build a more complex picture and gain a better understanding of these medically important phenomena. Our results demonstrate the significance of both physical and biochemical interactions in biofilm formation and bacterial infections and provided further evidence of the interconnections of chemotaxis and bacterial communication. I think that the future of science is not simply collecting more and more new but separate pieces of information about our world. Instead, I believe in gaining a more genuine understanding of the complexity of life by looking deeper into the connections and interactions between the known physical, chemical and biological processes. I really hope that our work is one small, but valuable step towards this holistic approach of scientific research.

Bibliography

[1] P.G. Falkowski. Tracing oxygen's imprint on earth's metabolic evolution. *Science*, 311(5768):1724–1725, 2006.

[2] R.D. Bardgett, C. Freeman, and N.J. Ostle. Microbial contributions to climate change through carbon cycle feedbacks. *The ISME Journal*, 2(8):805–814, 2008.

[3] P.J. Turnbaugh, R.E. Ley, M. Hamady, C.M. Fraser-Liggett, R. Knight, and J.I. Gordon. The human microbiome project. *Nature*, 449(7164):804–810, 2007.

[4] J.A. Shapiro. Thinking about bacterial populations as multicellular organisms. *Annu. Rev. Microbiol.*, 52:81–104, 1998.

[5] E.M. Purcell. Life at Low Reynolds Number. *Am. J. Phys.*, 45:3–11, 1977.

[6] E. Leifson. Staining, shape and arrangement of bacterial flagella. *J. Bacteriol.*, 62 (4):377–389, 1951.

[7] C. Li, A. Motaleb, M. Sal, S.F. Goldstein, and N.W. Charon. Spirochete periplasmic flagella and motility. *J. Mol. Microbiol. Biotechnol.*, 2(4):345–354, 2000.

[8] D.B. Kearns. A field guide to bacterial swarming motility. *Nat. Rev. Microbiol.*, 8 (9):634–644, 2010.

[9] H.C. Berg. *E. coli in Motion.* Springer-Verlag, 2003.

[10] H.C. Berg and R.A. Anderson. Bacteria swim by rotating their flagellar filaments. *Nature*, 245(5425):380–382, 1973.

[11] H.C. Berg. The rotary motor of bacterial flagella. *Annu. Rev. Biochem.*, 72(1): 19–54, 2003.

[12] S.H. Larsen, J. Adler, J.J. Gargus, and R.W. Hogg. Chemomechanical Coupling without ATP: The Source of Energy for Motility and Chemotaxis in Bacteria. *Proc. Nat. Acad. Sci. USA*, 71(4):1239–1243, 1974.

[13] M.D. Manson, P. Tedesco, H.C. Berg, F.M. Harold, and C. Van der Drift. A protonmotive force drives bacterial flagella. *Proc. Natl. Acad. Sci. USA*, 74(7): 3060–3064, 1977.

[14] C.V. Gabel and H.C. Berg. The speed of the flagellar rotary motor of Escherichia coli varies linearly with protonmotive force. *Proc. Natl. Acad. Sci. USA*, 100(15): 8748–8751, 2003.

[15] H.C. Berg and D.A Brown. Chemotaxis in Escherichia coli analysed by three-dimensional tracking. *Nature*, 239(5374):500–504, 1972.

[16] H.C. Berg. *Random Walks in Biology.* Princeton University Press, Princeton, 1993.

[17] K.V. Thimann and G.M. Curry. Phototropism and phototaxis. *Comp. Biochem.*, 1:243–306, 1960.

[18] J. Adler. Chemotaxis in Bacteria. *Science*, 153:708–715, 1966.

[19] R. Blakemore. Magnetotactic bacteria. *Science*, 190(4212):377–379, 1975.

[20] D.-P. Hader. New trends in photobiology: Ecological consequences of photomovement in microorganisms. *J. Photoch. Photobio. B*, 1(4):385–414, 1988.

[21] B.L. Taylor, I.B. Zhulin, and M.S. Johnson. Aerotaxis and other energy-sensing behavior in bacteria. *Annu. Rev. Microbiol.*, 53:103–128, 1999.

[22] J.P. Armitage. Bacterial tactic responses. *Adv. Microb. Physiol.*, 41:229–289, 1999.

[23] H. Salman, A. Zilman, C. Loverdo, M. Jeffroy, and A. Libchaber. Solitary Modes of Bacterial Culture in a Temperature Gradient. *Phys. Rev. Lett.*, 97(11):118101, 2006.

[24] R.W. Harvey, L.H. George, R.L. Smith, and D.R. LeBlanc. Transport of microspheres and indigenous bacteria through a sandy aquifer: results of natural-and forced-gradient tracer experiments. *Environ. Sci.Technol.*, 23(1):51–56, 1989.

[25] M.C.M. Van Loosdrecht, J. Lyklema, W. Norde, and A.J.B. Zehnder. Influence of Interfaces on Microbial Activity. *Microbiol. Rev.*, 54(1):75–87, 1990.

[26] H.C. Berg and L. Turner. Chemotaxis of bacteria in glass capillary arrays - Escherichia coli, motility, microchannel plate, and light scattering. *Biophys. J.*, 58(4): 919–930, 1990.

[27] J.T. Gannon, V.B. Manilal, and M. Alexander. Relationship between Cell Surface Properties and Transport of Bacteria through Soil. *Appl. Environ. Microbiol.*, 57 (1):190–193, 1991.

[28] G. Harkes, J. Dankert, and J. Feijen. Bacterial migration along solid surfaces. *Appl. Environ. Microbiol.*, 58(5):1500–1505, 1992.

[29] K. Maeda, Y. Imae, J.-I. Shioi, and F. Oosawa. Effect of temperature on motility and chemotaxis of Escherichia coli. *J. Bacteriol.*, 127(3):1039–1046, 1976.

[30] J.R. Lawrence, P.J. Delaquis, D.R. Korber, and D.E. Caldwell. Behavior of Pseudomonas fluorescens within the hydrodynamic boundary layers of surface microenvironments. *Microb. Ecol.*, 14(1–14), 1987.

[31] P. Frymier, R.M. Ford, H.C. Berg, and P. Cummings. Three-dimensional tracking of motile bacteria near a solid planar surface. *Proc. Nat. Acad. Sci. USA*, 92: 6195–6199, 1995.

[32] M.A.-S. Vigeant and R.M. Ford. Interactions between motile Escherichia coli and glass in media with various ionic strengths, as observed with a three-dimensional tracking microscope. *Appl. Environ. Microbiol.*, 63:3474–3479, 1997.

[33] P.C. Hiemenz and R. Rajagopalan. *Principles of colloid and surface chemistry.* Marcel Dekker, Inc., New York, N.Y., 3rd ed. edition, 1997.

[34] M.A.-S. Vigeant, R.M. Ford, M. Wagner, and L.K. Tamm. Reversible and Irreversible Adhesion of Motile Escherichia coli Cells Analyzed by Total Internal Reflection Aqueous Fluorescence Microscopy. *Appl. Environ. Microbiol.*, 68(6):2794–2801, 2002.

[35] A. Berke, L. Turner, H.C. Berg, and E. Lauga. Hydrodynamic Attraction of Swimming Microorganisms by Surfaces. *Phys. Rev. Lett.*, 101(3):038102, 2008.

[36] G. Li and J. Tang. Accumulation of Microswimmers near a Surface Mediated by Collision and Rotational Brownian Motion. *Phys. Rev. Lett.*, 103(7):078101, 2009.

[37] G. Li, J. Bensson, L. Nisimova, D. Munger, P. Mahautmr, J.X. Tang, M.R. Maxey, and Y.V. Brun. Accumulation of swimming bacteria near a solid surface. *Phys. Rev. E*, 84(4):041932, 2011.

[38] C.E. Zobell and D.Q. Anderson. Observations on the multiplication of bacteria in different volumes of stored sea water and the influence of oxygen tension and solid surfaces. *Biol. Bull.*, 71:324–342, 1936.

[39] J.W. Costerton, K.J. Cheng, G.G. Geesey, T.I. Ladd, J.C. Nickel, M. Dasgupta, and T.J. Marrie. Bacterial Biofilms in Nature and Disease. *Annu. Rev. Microbiol.*, 41:435–464, 1987.

[40] J.W. Costerton, Z. Lewandowski, D.E. Caldwell, D.R. Korber, and H.M. Lappin-Scott. Microbial biofilms. *Annu. Rev. Microbiol.*, 49:711–745, 1995.

[41] R.M. Donlan. Biofilms: microbial life on surfaces. *Emerging infectious diseases*, 8 (9):881–890, 2002.

[42] C. Beloin, A. Roux, and J.M. Ghigo. Escherichia coli biofilms. *Current topics in microbiology and immunology*, 322:249–289, 2008.

[43] J.C. Conrad. Physics of bacterial near-surface motility using flagella and type IV pili: implications for biofilm formation. *Research in Microbiology*, 163:619–629, 2012.

[44] J.W. Costerton, P.S. Stewart, and E.P. Greenberg. Bacterial biofilms: a common cause of persistent infections. *Science*, 284(5418):1318–1322, 1999.

[45] T-F. C. Mah and G.A. O'Toole. Mechanisms of biofilm resistance to antimicrobial agents. *Trends Microbiol.*, 9(1):34–39, 2001.

[46] B.W. Trautner and R.O. Darouiche. Role of biofilm in catheter-associated urinary tract infection. *Am. J. Infect. Control*, 32(3):177–183, 2004.

[47] C.A. Fux, J.W. Costerton, P.S. Stewart, and P. Stoodley. Survival strategies of infectious biofilms. *Trends Microbiol.*, 13(1):34–40, 2005.

[48] T. Mattila-Sandholm and G. Wirtanen. Biofilm formation in the food industry - a review. *Food Rev. Int.*, 8:573–603, 1992.

[49] S.W. Borenstein. *Microbiologically influenced corrosion handbook*. Woodhead Publishing Limited, Cambridge, 1994.

[50] V. Schaller, C. Weber, C. Semmrich, E. Frey, and A. R. Bausch. Polar patterns of driven filaments. *Nature*, 467(7311):73–77, 2010.

[51] J.O. Kessler and M.F. Wojciechowski. *Collective behavior and dynamics of swimming bacteria in Bacteria as Multicellular Organisms.* Oxford University Press, New York, 1997.

[52] N.H. Mendelson, A. Bourque, K. Wilkening, K.R. Anderson, and J.C. Watkins. Organized cell swimming motions in Bacillus subtilis colonies: patterns of short-lived whirls and jets. *J. Bacteriol.*, 181(2):600–609, 1999.

[53] C. Dombrowski, L. Cisneros, S. Chatkaew, R.E. Goldstein, and J.O. Kessler. Self-Concentration and Large-Scale Coherence in Bacterial Dynamics. *Phys. Rev. Lett.*, 93:098103, 2004.

[54] I.D. Couzin, J. Krause, R. James, G.D. Ruxton, and N.R. Franks. Collective memory and spatial sorting in animal groups. *J. Theor. Biol.*, 218(1):1–11, 2002.

[55] T. Vicsek and A. Zafiris. Collective motion. *Phys. Rep.*, 517:71–140, 2012.

[56] X.L. Wu and A. Libchaber. Particle diffusion in a quasi-two-dimensional bacterial bath. *Phys. Rev. Lett.*, 84(13):3017–3020, 2000.

[57] M. Wu, J.W. Roberts, S. Kim, D.L. Koch, and M.P. Delisa. Collective Bacterial Dynamics Revealed Using a Three-Dimensional Population-Scale Defocused Particle Tracking Technique. *Appl. Environ. Microbiol.*, 72(7):4987–4994, 2006.

[58] A. Sokolov, R. Goldstein, F. Feldchtein, and I. Aranson. Enhanced mixing and spatial instability in concentrated bacterial suspensions. *Phys. Rev. E*, 80(3):031903, 2009.

[59] A. Sokolov, I. Aranson, J. Kessler, and R. Goldstein. Concentration Dependence of the Collective Dynamics of Swimming Bacteria. *Phys. Rev. Lett.*, 98(15):158102, 2007.

[60] G. Gregoire and H. Chate. Onset of collective and cohesive motion. *Phys. Rev. Lett.*, 92(2):025702, 2004.

[61] J.P. Hernandez-Ortiz, C.G. Stoltz, and M.D. Graham. Transport and Collective Dynamics in Suspensions of Confined Swimming Particles. *Phys. Rev. Lett.*, 95(20): 204501, 2005.

[62] I. Aranson, A. Sokolov, J. Kessler, and R. Goldstein. Model for dynamical coherence in thin films of self-propelled microorganisms. *Phys. Rev. E*, 75(4):040901, 2007.

[63] A. Baskaran and M.C. Marchetti. Statistical mechanics and hydrodynamics of bacterial suspensions. *Proc. Nat. Acad. Sci. USA*, 106(37):15567–15572, 2009.

[64] J. Dunkel, S. Heidenreich, K. Drescher, H.H. Wensink, M. Bar, and R. Goldstein. Fluid dynamics of bacterial turbulence. *Phys. Rev. Lett.*, 110(22):228102, 2013.

[65] L. Angelani, R. Di Leonardo, and G. Ruocco. Self-starting micromotors in a bacterial bath. *Phys. Rev. Lett.*, 102(4):048104, 2009.

[66] R. Di Leonardo, L. Angelani, D. Dell'Arciprete, G. Ruocco, V. Iebba, S. Schippa, M.P. Conte, F. Mecarini, F. De Angelis, and E. Di Fabrizio. Bacterial ratchet motors. *Proc. Nat. Acad. Sci. USA*, 107(21):9541–9545, 2010.

[67] A. Sokolov, M.M. Apodaca, B.A. Grzybowski, and I.S. Aranson. Swimming bacteria power microscopic gears. *Proc. Nat. Acad. Sci. USASA*, 107(3):969–974, 2010.

[68] B. Kaehr and J.B. Shear. High-throughput design of microfluidics based on directed bacterial motility. *Lab Chip*, 9(18):2632–2637, 2009.

[69] B.L. Bassler. Small Talk: Cell-to-Cell Communication in Bacteria. *Cell*, 109:421–424, 2002.

[70] B.L. Bassler and R. Losick. Bacterially speaking. *Cell*, 125(2):237–246, 2006.

[71] R.M. Macnab and D.E. Koshland. The gradient-sensing mechanism in bacterial chemotaxis. *Proc. Nat. Acad. Sci. USA*, 69(9):2509–2512, 1972.

[72] T.W. Grebe and J. Stock. Bacterial chemotaxis: The five sensors of a bacterium. *Curr. Biol.*, 8(5):R154–R157, 1998.

[73] J.R. Maddock and L. Saphiro. Polar location of the chemoreceptor complex in the Escherichia coli cell. *Science*, 259:1717–1723, 1993.

[74] V. Sourjik. Receptor clustering and signal processing in E coli chemotaxis. *Trends Microbiol.*, 12(12):569–576, 2004.

[75] M.S. Springer, M.F. Goy, and J. Adler. Protein methylation in behavioral control mechanisms and in signal transduction. *Nature*, 280:279–284, 1979.

[76] M. Eisenbach. Signal transduction in bacterial chemotaxis. *Mod. Cell. Biol.*, 10: 137–208, 1991.

[77] M. Eisenbach. Control of bacterial chemotaxis. *Mol. Microbiol.*, 20(5):903–910, 1996.

[78] J.J. Falke, R.B. Bass, S.L. Butler, S.A. Chervitz, and M.A. Danielson. The two-component signaling pathway of bacterial chemotaxis: a molecular view of signal transduction by receptors, kinases, and adaptation enzymes. *Annu. Rev. Cell Dev. Biol.*, 13:457–512, 1997.

[79] M. Welch, K. Oosawa, S. Aizawa, and M. Eisenbach. Phosphorylation-dependent binding of a signal molecule to the flagellar switch of bacteria. *Proc. Natl. Acad. Sci. USA*, 90(19):8787–8791, 1993.

[80] U. Alon, L. Camarena, M.G. Surette, B. Aguera y Arcas, Y. Liu, S. Leibler, and J.B. Stock. Response regulator output in bacterial chemotaxis. *EMBO J.*, 17(15): 4238–4248, 1998.

[81] J.F. Hess, K. Oosawa, N. Kaplan, and M.I. Simon. Phosphorylation of three proteins in the signaling pathway of bacterial chemotaxis. *Cell*, 53(1):79–87, 1988.

[82] E.G. Ninfa, A. Stock, S. Mowbray, and J. Stock. Reconstitution of the bacterial chemotaxis signal transduction system from purified components. *J. Biol. Chem.*, 266(15):9764–9770, 1991.

[83] K.A. Borkovich, L.A. Alex, and M.I. Simon. Attenuation of sensory receptor signaling by covalent modification. *Proc. Natl. Acad. Sci. USA*, 89(15):6756–6760, 1992.

[84] S. Pandya, P. Iyer, V. Gaitonde, T. Parekh, and A. Desai. Chemotaxis of Rhizobium sp.S2 towards Cajanus cajan root exudate and its major components. *Curr. Microbiol.*, 38(4):205–209, 1999.

[85] R. Stocker, J.R. Seymour, A. Samadani, D.E. Hunt, and M.F. Polz. Rapid chemotactic response enables marine bacteria to exploit ephemeral microscale nutrient patches. *Proc. Nat. Acad. Sci. USA*, 105:4209–4214, 2008.

[86] G. Pandey and R.K. Jain. Bacterial Chemotaxis toward Environmental Pollutants: Role in Bioremediation. *Appl. Environ. Microbiol.*, 68(12):5789–5795, 2002.

[87] R. Freter and P.C.M. O'Brien. The role of chemotaxis in the association of motile bacteria with intestinal mucosa: Chemotactic responses of Vibrio cholerae and description of motile non-chemotactic mutants. *Infect. Immun.*, 34:215–221, 1981.

[88] M.S. Pittman, M. Goodwin, and D.J. Kelly. Chemotaxis in the human gastric pathogen Helicobacter pylori: different roles for CheW and the three CheV paralogues, and evidence for CheV2 phosphorylation. *Microbiology*, 147:2493–2504, 2001.

[89] S.M. Butler and A. Camilli. Both chemotaxis and net motility greatly influence the infectivity of Vibrio cholerae. *Proc. Natl. Acad. Sci. USA*, 101:5018–5023, 2004.

[90] K. Terry, S.M. Williams, L. Connolly, and K.M. Ottemann. Chemotaxis Plays Multiple Roles during Helicobacter pylori Animal Infection. *Infect. Immun.*, 73: 803–811, 2005.

[91] T. Bansal, D. Englert, J. Lee, M. Hegde, T.K. Wood, and A. Jayaraman. Differential Effects of Epinephrine, Norepinephrine, and Indole on Escherichia coli O157:H7 Chemotaxis, Colonization, and Gene Expression. *Infect. Immun.*, 75:4597–4607, 2007.

[92] B.L. Bassler. How bacteria talk to each other: regulation of gene expression by quorum sensing. How bacteria talk to each other: regulation of gene expression by quorum sensing. *Curr. Opin. Microbiol.*, 2(6):582–587, 1999.

[93] C. Fuqua, M.R. Parsek, and E.P. Greenberg. Regulation of gene expression by cell-to-cell communication: acyl-homoserine lactone quorum sensing. *Annu. Rev. Genet.*, 35:439–468, 2001.

[94] C.M. Waters and B.L. Bassler. Quorum Sensing: Cell-to-Cell Communication in Bacteria. *Annu. Rev. Cell Dev. Biol.*, 21:319–346, 2005.

[95] K.B. Xavier and B.L. Bassler. Interference with AI-2-mediated bacterial cell-cell communication. *Nature*, 437(7059):750–753, 2005.

[96] K.F. Chater and S. Horinouchi. Signalling early developmental events in two highly diverged Streptomyces species. *Mol. Microbiol.*, 48:9–15, 2003.

[97] E.C. Pesci, J.B. Milbank, J.P. Pearson, S. McKnight, A.S. Kende, E.P. Greenberg, and B.H. Iglewski. Quinolone signaling in the cell-to-cell communication system of Pseudomonas aeruginosa. *Proc. Natl. Acad. Sci. USA*, 96:11229–11234, 1999.

[98] A.B. Flavier, S.J. Clough, M.A. Schell, and T.P. Denny. Identification of 3-hydroxypalmitic acid methyl ester as a novel autoregulator controlling virulence in Ralstonia solanacearum. *Mol. Microbiol.*, 26:251–259, 1997.

[99] M.T. Holden, S. Ram Chhabra, R. de Nys, P. Stead, N.J. Bainton, P.J. Hill, M. Manefield, N. Kumar, M. Labatte, D. England, S. Rice, M. Givskov, G.P. Salmond, G.S. Stewart, B.W. Bycroft, S. Kjelleberg, and P. Williams. Quorum-sensing cross talk: isolation and chemical characterization of cyclic dipeptides from Pseudomonas aeruginosa and other gram-negative bacteria. *Mol. Microbiol.*, 33(6): 1254–1266, 1999.

[100] G.P.C. Salmond, B.W. Bycroft, G.S.A.B. Stewart, and P. Williams. The bacterial enigma: cracking the code of cell-cell communication. *Mol. Microbiol.*, 16:615–624, 1995.

[101] W.C. Fuqua, S.C. Winans, and E.P. Greenberg. Census and consensus in bacterial ecosystems: the LuxR-LuxI family of quorum sensing transcriptional regulators. *Annu. Rev. Microbiol.*, 50:727–751, 1996.

[102] A.M. Hardman, G.S.A.B. Stewart, and P. Williams. Quorum sensing and the cell-cell communication dependent regulation of gene expression in pathogenic and non-pathogenic bacteria. *Antony van Leeuwenhoek J. Microbiol.*, 74:199–210, 1998.

[103] G.M. Dunny and S.C. Winans. *Cell-cell signaling in bacteria.* Washington, DC: American Society of Microbiology Press., 1999.

[104] B.M.M. Ahmer. Cell-to-cell signalling in Escherichia coli and Salmonella enterica. *Mol. Microbiol.*, 52(4):933–945, 2004.

[105] R. Houdt, A. Aertsen, P. Moons, K. Vanoirbeek, and C.W. Michiels. N-acyl-L-homoserine lactone signal interception by Escherichia coli. *Fems Microbiol. Lett.*, 256:83–89, 2006.

[106] J. Lee, T. Maeda, S.H. Hong, and T.K. Wood. Reconfiguring the Quorum-Sensing Regulator SdiA of Escherichia coli To Control Biofilm Formation via Indole and N-Acylhomoserine Lactones. *Appl. Environ. Microbiol.*, 75(6):1703–1716, 2009.

[107] D.L. Englert, M.D. Manson, and A. Jayaraman. Flow-Based Microfluidic Device for Quantifying Bacterial Chemotaxis in Stable, Competing Gradients. *Appl. Environ. Microbiol.*, 75(13):4557–4564, 2009.

[108] T.R. De Kievit and B.H. Iglewski. Bacterial Quorum Sensing in Pathogenic Relationships. *Infect. Immun.*, 68:4839–4849, 2000.

[109] K. Winzer and P. Williams. Quorum sensing and the regulation of virulence gene expression in pathogenic bacteria. *Int. J. Med. Microbiol.*, 291:131–143, 2001.

[110] R.S. Smith and B.H. Iglewski. P. aeruginosa quorum-sensing systems and virulence. *Curr. Opin. Microbiol.*, 6:56–60, 2003.

[111] J.E. Keymer, P. Galajda, C. Muldoon, S. Park, and R.H. Austin. Bacterial metapopulations in nanofabricated landscapes. *Proc. Nat. Acad. Sci. USA*, 103 (46):17290–17295, 2006.

[112] G.M. Whitesides. The 'right' size in nanobiotechnology. *Nat. Biotech.*, 21(10): 1161–1165, 2003.

[113] D.B. Weibel, W.R. DiLuzio, and G.M. Whitesides. Microfabrication meets microbiology. *Nat. Rev. Microbiol.*, 5(3):209–218, 2007.

[114] J.C. McDonald, D.C. Duffy, J.R. Anderson, D.T. Chiu, H. Wu, O.J.A. Schueller, and G.M. Whitesides. Fabrication of microfluidic systems in poly(dimethylsiloxane). *Electrophoresis*, 21:27–40, 2000.

[115] G.M. Whitesides, E. Ostuni, S. Takayama, X. Jiang, and D.E. Ingber. Soft lithography in biology and biochemistry. *Ann. Rev. Biomed. Eng.*, 3:335–373, 2001.

[116] T. Ahmed, T.S. Shimizu, and R. Stocker. Microfluidics for bacterial chemotaxis. *Integr. Biol.*, 2(11-12):604, 2010.

[117] H. Mao, P.S. Cremer, and M.D. Manson. A sensitive, versatile microfluidic assay for bacterial chemotaxis. *Proc. Natl. Acad. Sci. USA*, 100(9):5449–5454, 2003.

[118] L.M. Lanning, R.M. Ford, and T. Long. Bacterial chemotaxis transverse to axial flow in a microfluidic channel. *Biotechnol. Bioeng.*, 100(4):653–663, 2008.

[119] R. Stocker, J.R. Seymour, A. Samadani, D.E. Hunt, and M.F. Polz. Rapid chemotactic response enables marine bacteria to exploit ephemeral microscale nutrient patches. *Proc. Nat. Acad. Sci. USA*, 105(11):4209–4214, 2008.

[120] H. Jeon, Y. Lee, S. Jin, S. Koo, C.S. Lee, and J.Y. Yoo. Quantitative analysis of single bacterial chemotaxis using a linear concentration gradient microchannel. *Biomed. Microdevices*, 11(5):1135–1143, 2009.

[121] T. Ahmed and R. Stocker. Experimental Verification of the Behavioral Foundation of Bacterial Transport Parameters Using Microfluidics. *Biophys. J.*, 95(9):4481–4493, 2008.

[122] T. Kim, M. Pinelis, and M.M. Maharbiz. Generating steep, shear-free gradients of small molecules for cell culture. *Biomed. Microdevices*, 11(1):65–73, 2009.

[123] J.J. VanDersarl, A.M. Xu, and N.A. Melosh. Rapid spatial and temporal controlled signal delivery over large cell culture areas. *Lab Chip*, 11(18):3057–3063, 2011.

[124] J. Diao, L. Young, S. Kim, E.A. Fogarty, S.M. Heilman, P. Zhou, M.L. Shuler, M. Wu, and M.P. DeLisa. A three-channel microfluidic device for generating static linear gradients and its application to the quantitative analysis of bacterial chemotaxis. *Lab Chip*, 6(3):381–388, 2006.

[125] S.Y. Cheng, S. Heilman, M. Wasserman, S. Archer, M.L. Shuler, and M. Wu. A hydrogel-based microfluidic device for the studies of directed cell migration. *Lab Chip*, 7(6):763–769, 2007.

[126] T. Ahmed, T.S. Shimizu, and R. Stocker. Bacterial chemotaxis in linear and nonlinear steady microfluidic gradients. *Nano Lett.*, 10(9):3379–3385, 2010.

[127] Y. Zhou and Q. Lin. Microfluidic flow-free generation of chemical concentration gradients. *Sens. Actuators B*, 190:334–341, 2014.

[128] H. Wu, B. Huang, and R.N. Zare. Generation of complex, static solution gradients in microfluidic channels. *J. Am. Chem. Soc.*, 128:4194–4195, 2006.

[129] M. Kim and T. Kim. Diffusion-Based and Long-Range Concentration Gradients of Multiple Chemicals for Bacterial Chemotaxis Assays. *Anal. Chem.*, 82(22):9401–9409, 2010.

[130] G. Si, W. Yang, S. Bi, C. Luo, and Q. Ouyang. A parallel diffusion-based microfluidic device for bacterial chemotaxis analysis. *Lab Chip*, 12(7):1389–1394, 2012.

[131] Y. Xia and G.M. Whitesides. Soft Lithography. *Angew. Chem. Int. Ed.*, 37:550–575, 1998.

[132] A. del Campo and C. Greiner. SU-8: a photoresist for high-aspect-ratio and 3D submicron lithography. *J. Micromech. Microeng.*, 17:R81–R95, 2007.

[133] D. Qin, Y. Xia, and G.M. Whitesides. Soft lithography for micro- and nanoscale patterning. *Nat. Protoc.*, 5(3):491–502, 2010.

[134] B. Chueh, D. Huh, C.R. Kyrtsos, T. Houssin, N. Futai, and S. Takayama. Leakage-free bonding of porous membranes into layered microfluidic array systems. *Anal. Chem.*, 79(9):3504–3508, 2007.

[135] A.J. Wolfe, M.P. Conley, T.J. Kramer, and H.C. Berg. Reconstitution of signaling in bacterial chemotaxis. *J. Bacteriol.*, 169(5):1878–1885, 1987.

[136] M.P. Mayer. A new set of useful cloning and expression vectors derived from pBlue-Script. *Gene*, 163(1):41–46, 1995.

[137] B.J. Bachmann. *Escherichia coli and Salmonella typhimurium: cellular and molecular biology.*, chapter Derivations and genotypes of some mutant derivatives of Escherichia coli K-12., pages 1191–1219. American Society for Microbiology, 1987.

[138] R.S. Kumar, N. Ayyadurai, P. Pandiaraja, A.V. Reddy, Y. Venkateswarlu, O. Prakash, and N. Sakthivel. Characterization of antifungal metabolite produced by a new strain Pseudomonas aeruginosa PUPa3 that exhibits broad-spectrum antifungal activity and biofertilizing traits. *J. Appl. Microbiol.*, 98:145–154, 2005.

[139] C.T. Culbertson, S.C. Jacobson, and J.M. Ramsey. Diffusion coefficient measurements in microfluidic devices. *Talanta*, 56:365–373, 2002.

[140] J. Schindelin et al. Fiji: an open-source platform for biological-image analysis. *Nat. Methods*, 9:676–682, 2012.

[141] S.P. Strong, B. Freedman, W. Bialek, and R. Koberle. Adaptation and optimal chemotactic strategy for E. coli. *Phys. Rev. E*, 57(4):4604–4617, 1998.

[142] W.R. DiLuzio, L. Turner, M. Mayer, P. Garstecki, D.B. Weibel, H.C. Berg, and G.M. Whitesides. Escherichia coli swim on the right-hand side. *Nature*, 435:1271–1274, 2005.

[143] E. Lauga, W.R. DiLuzio, G.M. Whitesides, and H.A. Stone. Swimming in Circles: Motion of Bacteria near Solid Boundaries. *Biophys. J.*, 90(2):400–412, 2006.

[144] D. Giacché, T. Ishikawa, and T. Yamaguchi. Hydrodynamic entrapment of bacteria swimming near a solid surface. *Phys. Rev. E*, 82(5):056309, 2010.

[145] P. Galajda, J. Keymer, P. Chaikin, and R. Austin. A Wall of Funnels Concentrates Swimming Bacteria. *J. Bacteriol.*, 189(23):8704–8707, 2007.

[146] R. Mesibov and J. Adler. Chemotaxis toward amino acids in Escherichia coli. *J. Bacteriol.*, 112(1):315–326, 1972.

[147] T.S. Charlton, R. de Nys, A. Netting, N. Kumar, M. Hentzer, M. Givskov, and S. Kjelleberg. A novel and sensitive method for the quantification of N-3-oxoacyl homoserine lactones using gas chromatography-mass spectrometry: application to a model bacterial biofilm. *Environ. Microbiol.*, 2(5):530–541, 2000.

[148] A. Beare, R.J. For, L.W. Martin, and I.L. Lamont. Siderophore-mediated cell signalling in Pseudomonas aeruginosa: divergent pathways regulate virulence factor production and siderophore receptor synthesis. *Mol. Microbiol.*, 47(1):195–207, 2003.

[149] A. Stintzi, K. Evans, J.M. Meyer, and K. Poole. Quorum-sensing and siderophore biosynthesis in Pseudomonas aeruginosa: lasR/lasI mutants exhibit reduced pyoverdine biosynthesis. *Fems Microbiol. Lett.*, 166(2):341–345, 1998.

[150] S.S. Baron and J.J. Rowe. Antibiotic action of pyocyanin. *Antimicrob. Agents Chemother.*, 20(6):814–820, 1981.

[151] R. Xiao and W.S. Kisaalita. Purification of Pyoverdines of Pseudomonas fluorescens 2-79 by Copper-Chelate Chromatography. *Appl. Environ. Microbiol.*, 61(11):3769–3774, 1995.

[152] J.M. Henke and B.L. Bassler. Bacterial social engagements. *Trends Cell Biol.*, 14 (11):648–656, 2004.

[153] M.B. Miller and B.L. Bassler. Quorum sensing in bacteria. *Annu. Rev. Microbiol.*, 55:165–99, 2001.

[154] J.F. Linares, I. Gustafsson, F. Baquero, and J.L. Martinez. Antibiotics as intermicrobial signaling agents instead of weapons. *Proc. Nat. Acad. Sci. USA*, 103(51): 19484–19489, 2006.

[155] M. Kleerebezem, L.E. Quadri, O.P. Kuipers, and W.M. de Vos. Quorum sensing by peptide pheromones and two-component signal-transduction systems in Gram-positive bacteria. *Mol. Microbiol.*, 24(5):895–904, 1997.

[156] S.K. Kim, D. Kaiser, and A. Kuspa. Control of cell density and pattern by intercellular signaling in Myxococcus development. *Annu. Rev. Microbiol.*, 46:117–139, 1992.

[157] J.A. Leigh and D.L. Coplin. Exopolysaccharides in plant-bacterial interactions. *Annu. Rev. Microbiol.*, 46:307–346, 1992.

[158] Jin-Hyung Lee and Jintae Lee. Indole as an intercellular signal in microbial communities. *FEMS Microbiology Reviews*, January 2010.

[159] S.G. Charati and S.A. Stern. Diffusion of Gases in Silicone Polymers: Molecular Dynamics Simulations. *Macromolecules*, 31(16):5529–5535, 1998.

[160] E. Leclerc, Y. Sakai, and T. Fujii. Cell Culture in 3-Dimensional Microfluidic Structure of PDMS (polydimethylsiloxane). *Biomed. Microdevices*, 5(2):109–114, 2003.

[161] S. Park, P.M. Wolanin, E.A. Yuzbashyan, H. Lin, N.C. Darnton, J.B. Stock, P. Silberzan, and R. Austin. Influence of topology on bacterial social interaction. *Proc. Nat. Acad. Sci. USA*, 100(24):13910–13915, 2003.

[162] W.W. Tso and J. Adler. Negative chemotaxis in Escherichia coli. *J. Bacteriol.*, 118 (2):560–576, 1974.

[163] D. Wang, X. Ding, and P.N. Rather. Indole can act as an extracellular signal in Escherichia coli. *J. Bacteriol.*, 183(14):4210–4216, 2001.

[164] J. Lee, A. Jayaraman, , and T.K. Wood. Indole is an inter-species biofilm signal mediated by SdiA. *BMC Microbiol.*, 7:42, 2007.

[165] A. Kobayashi, H. Hirakawa, T. Hirata, K. Nishino, and A. Yamaguchi. Growth phase-dependent expression of drug exporters in Escherichia coli and its contribution to drug tolerance. *J. Bacteriol.*, 188(16):5693–5703, 2006.

[166] E.L. Chant and D.K. Summers. Indole signalling contributes to the stable maintenance of Escherichia coli multicopy plasmids. *Mol. Microbiol.*, 63(1):35–43, 2007.

[167] M.T.G. Holden, S.R. Chhabra, R. de Nys, P. Stead, N.J. Bainton, P.J. Hill, M. Manefield, K. Kumar, M. Labatte, D. England, S. Rice, M. Givskov, G.P.C. Salmond, G.S.A.B. Stewart, B.W. Bycroft, S. Kjelleberg, and P. Williams. Quorum-sensing cross talk: isolation and chemical characterization of cyclic dipeptides from Pseudomonas aeruginosa and other Gram-negative bacteria. *Mol. Microbiol.*, 33: 1254–1266, 1999.

[168] Y. Tashiro, S. Ichikawa, T. Nakajima-Kambe, H. Uchiyama, and N. Nomura. Pseudomonas Quinolone Signal Affects Membrane Vesicle Production in not only Gram-Negative but also Gram-Positive Bacteria. *Microbes Environ.*, 25(2):120–125, 2010.